Progress of Theoretical Physics, Vol. 108, No. 5, November 2002

Symmetry Breaking and Bifurcations in the Periodic Orbit Theory. II

— Spheroidal Cavity —

Alexander G. Magner,[1,2,3] Ken-ichiro Arita,[4] Sergey N. Fedotkin[2,3] and Kenichi Matsuyanagi[5]

[1]*Research Center for Nuclear Physics, Osaka University, Ibaraki 567-0047, Japan*
[2]*Institute for Nuclear Research, 03680 Prospekt Nauki 47, Kiev-28, Ukraine*
[3]*Institute for Theoretical Physics, University of Regensburg, D-93040 Regensburg, Germany*
[4]*Department of Physics, Nagoya Institute of Technology, Nagoya 466-8555, Japan*
[5]*Department of Physics, Graduate School of Science, Kyoto University, Kyoto 606-8502, Japan*

(Received August 5, 2002)

We derive a semiclassical trace formula for the level density of a three-dimensional spheroidal cavity. To overcome the divergences and discontinuities occurring at bifurcation points and in the spherical limit, the trace integrals over the action-angle variables are performed using an improved stationary phase method. The resulting semiclassical level density oscillations and shell energies are in good agreement with quantum-mechanical results. We find that the births of three-dimensional orbits through the bifurcations of planar orbits in the equatorial plane lead to considerable enhancement of the shell effect for superdeformed shapes.

§1. Introduction

The periodic orbit theory (POT)[1)–10)] is a nice tool for studying the correspondence between classical and quantum mechanics and, in particular, the interplay of deterministic chaos and quantum-mechanical behavior. Also, for systems with integrable or mixed classical non-linear dynamics, the POT leads to a deeper understanding of the origin of shell structure in finite fermion systems, such as nuclei,[8),11)–13)] metallic clusters,[14)–16)] and mesoscopic semiconductors.[17)–21)] Bifurcations of periodic orbits may play significant roles, e.g., in connection with superdeformations of atomic nuclei,[8),9),12),22)–24)] and were recently shown to affect the quantum oscillations observed in the magneto-conductance of mesoscopic devices.[19),20)] This phenomenon is observed for some control parameters (like the shape, magnetic field, etc.) of the potential well, for which the orbits bifurcate and new types of periodic orbits emerge from the original ones. Examples can be found, e.g., in elliptic billiard and spheroidal cavity systems.[8),9),12),23)–28)] In elliptic billiard systems, short diametric orbits with repetitions bifurcate at certain values of the deformation parameter, and new orbits with hyperbolic caustics (butterfly-shaped orbit, etc.) emerge from them. In spheroidal cavity systems, periodic orbits in the equatorial plane bifurcate, and new three-dimensional orbits emerge.

The semiclassical trace formulae connect the quantum mechanical density of states with a sum over the periodic orbits of the classical system.[1)–4)] In these formulae, divergences arise at critical points where bifurcations of periodic orbits occur or where symmetry breaking (or restoring) transitions take place. At these points, the standard stationary phase method (SSPM),[*)] used in the semiclassical evaluation of the trace integrals, breaks down. Various ways of avoiding these divergences have been studied,[3),5),29)] some of them employing uniform approximations.[29)–37)] Here we employ an improved stationary-phase method (ISPM) for the evaluation of the trace integrals in the phase-space representation, which we have derived for elliptic billiards[28)] and very recently for spheroidal cavities.[24)]

The singularities of the SSPM near the bifurcation points are due to the peculiarities of its asymptotic expansions. In the ISPM,[24),28)] the catastrophe integrals[38),39)] are evaluated more exactly within the finite integration limits in the phase-space trace formula,[3),5),9),24),28),40)] and it is possible to overcome the singularity problem due to bifurcations, which occur when the stationary points lie near the ends of the integration region in the action-angle variables. We can also take into account the stationary points outside the classically accessible region ("ghost orbits").[5)] This method is particularly useful for integrable systems in which integration limits are easily obtained. This theory is developed in Ref. 28) for the case of the bifurcations through which periodic orbit families with maximal degeneracy emerge from orbits with smaller degeneracy. The essential difference between the method presented in this paper and that with the uniform approximation of Refs. 32) and 35) is that we improve the calculation of the *angle* part of the phase-space trace integral for the orbits with smaller degeneracies. Taking an elliptic billiard system as an example, we have applied the ISPM to the integration over the angle variable for short diametric orbits and derived an improved trace formula that is continuous through all bifurcation points, including the circular limit and the separatrix. We then showed that significant enhancements of the shell effect in level densities and shell structure energies occur at deformations near the bifurcation points. Away from the bifurcation points, our result reduces to the extended Gutzwiller trace formula,[4),8)–10)] and for the leading-order families of periodic orbits, it is identical to that of Berry and Tabor.[5)]

The major purpose of this paper is to extend our semiclassical ISPM to the case of a three-dimensional (3D) spheroidal cavity,[24)] which may be taken as a simple (highly idealized) model for a heavy deformed nucleus[8),11)] or a deformed metallic cluster,[14),15)] and to specify the role of periodic orbit bifurcations in the shell structure responsible for superdeformations. Although the spheroidal cavity system is integrable, it exhibits all the difficulties mentioned above (i.e., symmetry breaking and bifurcations), and therefore it provides an exemplary case study of a non-trivial 3D system. We apply the ISPM to the bifurcating orbits and succeed in reproducing the superdeformed shell structure in terms of the POT, while observing a considerable enhancement of the shell effect near the bifurcation points.

[*)] In this paper, SSPM is understood as the standard stationary phase method and its extension to continuous symmetries.[3)–5),7)]

§2. Classical mechanics for the spheroidal cavity

The semiclassical trace formulas for the oscillating part of the level density for a spheroidal cavity are determined from the characteristic properties of the classical periodic families.[8),9),22)–27)] This section presents definitions and solutions for the classical mechanical description of the spheroidal cavity, following Refs. 8), 9), 23) and 27). They will be used for the semiclassical derivations of the trace formulas improved at the bifurcation points. We shall pay special attention to the 3D periodic orbits that emerge through bifurcations and play important roles as the semiclassical origin of superdeformed shell structure.[8),23),27)]

2.1. *General periodic-orbit formalism*

We characterize the spheroid by the ratio of its semi-axes $\eta = b/a$, keeping its volume fixed, and consider the prolate case with $\eta > 1$, where the major axis coincides with the symmetry axis. We first transform the Cartesian coordinates (x, y, z) into the usual cylindrical coordinates (ρ, z, φ), where $\rho = \sqrt{x^2 + y^2}$, which are expressed in terms of the spheroidal coordinates (u, v, φ) as

$$\rho = \zeta \cos u \sinh v, \quad z = \zeta \sin u \cosh v, \quad \zeta = \sqrt{b^2 - a^2}, \tag{2·1}$$

with

$$-\frac{\pi}{2} \le u \le \frac{\pi}{2}, \quad 0 \le v < \infty, \quad 0 \le \varphi \le 2\pi. \tag{2·2}$$

The values of $\pm\zeta$ define the positions of the foci of the spheroid lying on the z-axis. Taking into account the volume conservation condition $a^2 b = R^3$, we have $b = R\eta^{2/3}$ and $a = R\eta^{-1/3}$. As is well known, the Hamilton-Jacobi equations separate in the coordinates (u, v, φ) for a spheroidal cavity.

In the Hamilton-Jacobi formalism, the classical dynamics are determined by the partial actions. In the spheroidal coordinates, these are given by

$$I_u = \frac{p\zeta}{\pi} \int_{-u_c}^{u_c} du \sqrt{\sigma_1 - \sin^2 u - \frac{\sigma_2}{\cos^2 u}}, \tag{2·3a}$$

$$I_v = \frac{p\zeta}{\pi} \int_{v_c}^{v_b} dv \sqrt{\cosh^2 v - \sigma_1 - \frac{\sigma_2}{\sinh^2 v}}, \tag{2·3b}$$

$$I_\varphi = |l_z| = p\zeta\sqrt{\sigma_2}, \tag{2·3c}$$

where l_z is the projection of the angular momentum onto the symmetry axis, and $p = \sqrt{2m\varepsilon}$, where m is the particle mass. In Eq. (2·3) we have introduced the new "action" variables σ_1 and σ_2 related to the turning points $-u_c$, u_c and v_c, v_b along the trajectory in the (u, v) coordinates; $u = u_c$ and $v = v_c$ are the (hyperbolic and elliptic) caustic surfaces,

$$\cosh v_c = \left\{ \frac{1}{2}(1 + \sigma_1) + \left[\frac{1}{4}(1 - \sigma_1)^2 + \sigma_2 \right]^{1/2} \right\}^{1/2}, \tag{2·4a}$$

$$\sin u_c = \left\{ \frac{1}{2}(1 + \sigma_1) - \left[\frac{1}{4}(1 - \sigma_1)^2 + \sigma_2 \right]^{1/2} \right\}^{1/2}, \tag{2·4b}$$

and $v = v_b$ is the spheroid boundary, given by $\cosh v_b = \eta/\sqrt{\eta^2-1}$. The condition that the kinetic energy must be positive determines the limits for the variables σ_1 and σ_2:

$$\sigma_1^- = \sigma_2 \le \sigma_1 \le \frac{\eta^2}{\eta^2-1} - \sigma_2\left(\eta^2-1\right) = \sigma_1^+,$$
$$\sigma_2^- = 0 \le \sigma_2 \le \frac{1}{\eta^2-1} = \sigma_2^+. \tag{2·5}$$

These inequalities together with the 2π intervals for the corresponding angle variables determine the tori of the classically accessible motion with the boundaries $\sigma_1^{\pm}(\sigma_2)$ and $\sigma_2^{\pm}$.

According to Eq. (2·3), the particle energy ε is a function of only the action variables I_u, I_v and I_φ, $\varepsilon = H\left(I_u, I_v, I_\varphi\right)$, due to the integrability of the system under consideration. These relations define the partial frequencies ω_u, ω_v and ω_φ through $\omega_j = \partial H/\partial I_j$. The periodicity conditions for the classical trajectories are significantly simplified in terms of the partial frequencies ω_j. Introducing the new variables κ and θ,

$$\kappa = \frac{\sin u_c}{\cosh v_c}, \quad \theta = \arcsin\left(\frac{\cosh v_c}{\cosh v_b}\right), \tag{2·6}$$

along with the energy ε in place of the partial actions I_u, I_v and I_φ (or σ_1 and σ_2), they read

$$\frac{\omega_u}{\omega_v} \equiv \frac{1}{2}\left[1 - \frac{\mathrm{F}(\theta,\kappa)}{\mathrm{F}(\kappa)}\right] = \frac{n_u}{n_v}, \tag{2·7a}$$
$$\frac{\omega_\varphi}{\omega_u} \equiv \frac{2}{\pi}\left[\left(1-\left(\frac{\kappa}{\bar\kappa}\right)^2\right)\left(1-\bar\kappa^2\right)\right]^{1/2}\left\{\Pi\left(\left(\frac{\kappa}{\bar\kappa}\right)^2,\kappa\right) - \mathrm{F}(\kappa)\right.$$
$$\left. + \left[\Pi\left(\bar\kappa^2,\kappa\right) - \Pi\left(\theta,\bar\kappa^2,\kappa\right)\right] \Big/ \left[1 - \frac{\mathrm{F}(\theta,\kappa)}{\mathrm{F}(\kappa)}\right]\right\} = \frac{n_\varphi}{n_u}. \tag{2·7b}$$

Here, n_u, n_v and n_φ are co-prime integers: $n_u = 1, 2, \cdots$; $n_v \ge 2n_u$; $n_v \ge 2n_\varphi$, $n_\varphi = 1, 2, \cdots$, and $\bar\kappa = \sqrt{\eta^2-1}/(\eta\sin\theta)$. F and Π are elliptic integrals of the 1st and 3rd kinds (see Appendix A for their definitions). The periodicity condition (2·7) relates $\kappa(\sigma_1,\sigma_2)$ and $\theta(\sigma_1,\sigma_2)$ for a given periodic orbit β to the integers n_u, n_v and n_φ, which, together with the number of repetitions M, define this orbit; i.e., $\beta = M(n_v, n_\varphi, n_u)$.

2.2. *Three-dimensional periodic orbits*

The 3D periodic orbits (3DPO) $M(n_v, n_\varphi, n_u)$ form two-parameter ($\mathcal{K} = 2$) families for a given energy ε, because the number $\mathcal{K}$ of free continuous parameters specifying an orbit with fixed energy and a given action is two.[8),9)] The condition for 3DPO is the existence of real roots (κ, θ) of Eq. (2·7). They appear at the deformation $\eta = \eta_{\mathrm{bif}}$ given by

$$\eta_{\mathrm{bif}} = \frac{\sin(\pi n_\varphi/n_v)}{\sin(\pi n_u/n_v)}, \quad (n_u = 1, 2, \cdots,\ n_v \ge 2n_\varphi + 1,\ n_\varphi = 2, 3, \cdots) \tag{2·8}$$

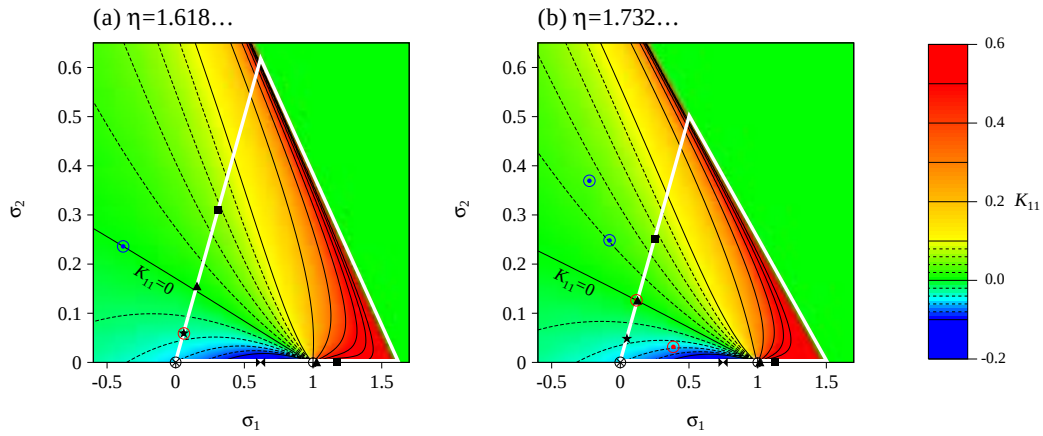

Fig. 1. The triangle of the classically accessible region determined by Eq. (2·5) is indicated by white lines in the (σ_1, σ_2) plane at the bifurcation deformations (a) $\eta = 1.618\ldots$ and (b) $\eta = \sqrt{3}$. The red and blue dots with the circles indicate the 3DPO stationary points inside (actually existing 3DPO) and outside ("ghost" 3DPO) of this triangle region, respectively. Several examples of the stationary points are indicated: on the $\sigma_2 = 0$ side, the short 2DPO (elliptic triangle, square, and hyperbolic "butterfly"); on the $\sigma_2 = \sigma_1$ side, the short EQPO (triangle, square, star and diameter (black crossed circle)). The long diameter (separatrix) is located at $(\sigma_1 = 1, \sigma_2 = 0)$. The color and contour curves indicate (in units of $p\zeta/\pi$) the curvature K_{11} defined by Eq. (3·14).

where $\kappa = 0$ and $\theta = \pi(1 - 2n_u/n_v)/2$, and exist for larger deformations $\eta > \eta_{\rm bif}$. These roots determine the caustics (the spheroid $v = v_c$ and the hyperboloids $u = \pm u_c$) of the periodic orbit $M(n_v, n_\varphi, n_u)$ through Eq. (2·6). These caustics are confocal to the boundary of the spheroid $v = v_b$.

Figure 1 displays the stationary points corresponding to the 3DPO for two bifurcation points $\eta_{\rm bif}$ given by (2·8). The physical tori region (2·5) in the variables σ_i is a triangle. At $\eta_{\rm bif} = 1.618\ldots$ (Fig. 1(a)), the stationary point for the 3DPO $(5, 2, 1)$ coincides with that for the star-shaped $(5, 2)$ orbit in the equatorial plane (discussed below) lying on the boundary with $\sigma_2 = \sigma_1$, and moves toward the inside of the physical tori region for larger deformations. At $\eta_{\rm bif} = \sqrt{3}$ (Fig. 1(b)), the stationary point for the 3DPO $(6, 2, 1)$ lies on the boundary side and coincides with that for triangular orbits in the equatorial plane. At these bifurcation deformations, the lengths of the 3DPO $(5, 2, 1)$ and $(6, 2, 1)$ coincide with those of the star $(5, 2)$ and the doubly repeated triangle $2(3, 1)$, respectively. Figure 2 illustrates some short 3DPO and their projections onto the equatorial plane.

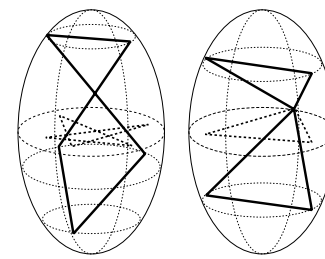

Fig. 2. Short 3D periodic orbits (5,2,1) and (6,2,1) bifurcated from the equatorial plane orbits (5,2) and 2(3,1), respectively. Their projections on the equatorial plane are also represented by thick-dashed lines.

2.3. *Orbits in the meridian plane*

Equations (2·7a) and (2·7b) have partial solutions for $\kappa(\sigma_1, \sigma_2)$ and $\theta(\sigma_1, \sigma_2)$ that correspond to the separate families of orbits, i.e. two-dimensional periodic orbits (2DPO), in the meridian planes (containing the symmetry axis z) and in the equatorial plane. First, we consider the special solutions of Eq. (2·7) corresponding to the two-parameter ($\mathcal{K} = 2$) 2DPO families in the meridian plane.[8),9)] For these orbits, $\sigma_2 = 0$ and σ_1 is in either of the regions

$$0 < \sigma_1 < 1, \qquad 1 < \sigma_1 < \frac{\eta^2}{\eta^2 - 1}, \tag{2·9}$$

for the hyperbolic 2DPO (with hyperbolic caustics $u = \pm u_c$) and the elliptic 2DPO (with elliptic caustics $v = v_c$), respectively. The periodicity condition (2·7b) becomes the identity $\omega_\varphi/\omega_u \equiv 1$ ($n_\varphi = 1$, $n_u = 1$), and θ is fixed by

$$\theta = \theta_h = \arcsin\left(\frac{\sqrt{\eta^2 - 1}}{\eta}\right), \qquad \theta = \theta_e = \arcsin\left(\frac{\sqrt{\eta^2 - 1}}{\kappa\eta}\right), \tag{2·10}$$

for the hyperbolic and elliptic 2DPO, respectively. For κ, we have only the condition Eq. (2·7a). This κ determines σ_1, and thus I_u and I_v ($I_\varphi = 0$ since $\sigma_2 = 0$), through

$$\kappa = \kappa_h = \sqrt{\sigma_1}, \qquad \kappa = \kappa_e = \frac{1}{\sqrt{\sigma_1}}, \tag{2·11}$$

for the hyperbolic and elliptic orbits, respectively.

Some examples of the hyperbolic and elliptic orbits lying along the triangular boundary side $\sigma_2 = 0$ are presented in Fig. 1 (see also their geometrical illustrations in Fig. 3). The hyperbolic and elliptic tori parts are separated by the separatrix point ($\sigma_1 = 1, \sigma_2 = 0$) related to the long diameter (see below). Another endpoint of the hyperbolic tori coincides with the stationary point ($\sigma_1 = \sigma_2 = 0$) for the diametric orbit in the equatorial plane. We can think of these hyperbolic and elliptic orbits as being periodic in the plane $\varphi = $ [const.], and we call them "meridian-plane periodic orbits".

For the elliptic case, a solution κ of Eq. (2·7) with $\theta = \theta_e(\kappa)$ exists for any $n_u = 1, 2, \cdots$ and $n_v \geq 2n_u + 1$, $(n_\varphi = n_u)$ for any deformation $\eta > 1$. Examples are

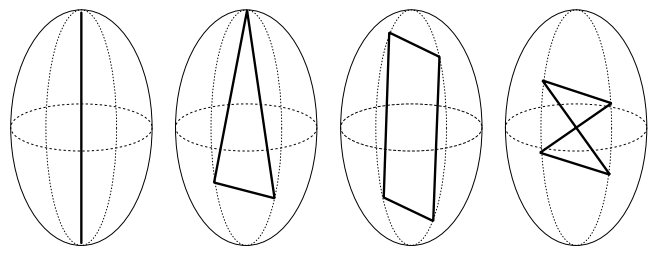

Fig. 3. Some short meridian-plane orbits in the prolate spheroidal cavity. From left to right: the isolated long diameter $(2, 1, 1)$, the elliptic triangular $(3, 1, 1)$, the elliptic rhomboidal $(4, 1, 1)$, the hyperbolic "butterfly" $(4, 2, 1)$.

the triangles $(n_v = 3, n_\varphi = 1, n_u = 1)$, the rhomboids $(4, 1, 1)$ and the star-shaped orbits $(5, 2, 2)$ as one-parameter families in the meridian plane. The root κ found from Eq. (2·7) gives the elliptic caustics with $u_c = \pi/2$ in Eq. (2·6) and the semi-axes $a_c = \zeta\sqrt{1-\kappa^2}/\kappa$ and $b_c = \zeta/\kappa$.

For the hyperbolic case, the solutions κ can be found for $n_u = 1, 2, 3, \cdots$ and even n_v $(n_v \geq 2(n_u + 1))$. In Fig. 1 the "butterfly" orbit $(4, 2, 1)$ is shown as an example. The families of these orbits appear for $\eta > \eta_{\rm bif}$ with

$$\eta_{\rm bif} = \left[\sin\left(\frac{\pi n_u}{n_v}\right)\right]^{-1}. \tag{2·12}$$

This is the deformation at which the diametric orbits $M(2, 1)$ with $M \geq 2$ in the equatorial plane bifurcate, and from these orbit emerge the hyperbolic orbits. Their hyperbolic caustics are expressed in terms of the root κ of Eqs. (2·7) and (2·6) with $v_c = 0$. The parameters a_c and b_c of these caustics are given by $a_c = \zeta\sqrt{1-\kappa^2}$ and $b_c = \zeta\kappa$.

2.4. *Orbits in the equatorial plane*

In the equatorial plane with $z = 0$, the separate families of regular polygons and diameters are the same as for a circular billiard system[3)] of radius a. The restriction $z = 0$ decreases the values of $\mathcal{K}$ to 1. The single parameter in this case corresponds to the angle of rotation of the polygons and the diameters about the symmetry axis z. Figure 4 illustrates the most important (shortest) equatorial-plane periodic orbits (EQPO): the diameters $M(n_v = 2, n_\varphi = 1)$, triangles $M(3, 1)$, squares $M(4, 1)$ and star-shaped orbits $M(5, 2)$. They satisfy, from inequalities (2·5),

$$\sigma_1 = \sigma_2, \qquad 0 \leq \sigma_2 \leq \frac{1}{\eta^2 - 1}. \tag{2·13}$$

Therefore their stationary points lie along the $\sigma_2 = \sigma_1$ side in the triangle, as indicated in Fig. 1.

The caustic parameters u_c and v_c for these families are defined by $u_c = 0$ and $v_c = \operatorname{arcsinh}[a\cos(\pi n_\varphi/n_v)/\zeta]$. The solutions of Eq. (2·7) for these orbits are $\kappa = 0$ and $\theta = \arcsin\sqrt{1 - \sin^2(\pi n_\varphi/n_v)/\eta^2}$.

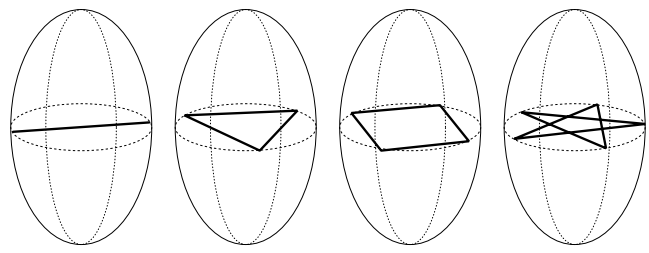

Fig. 4. Some short equatorial-plane orbits. From left to right: the short diameter $(2, 1)$, the triangular $(3, 1)$, the rhomboidal $(4, 1)$, and the star-shaped $(5, 2)$.

2.5. *Diametric orbits along the symmetry axis*

In the spheroidal cavity, there is also a diametric orbit along the z-axis (see Fig. 3). It is isolated ($\mathcal{K} = 0$), because we have two additional restrictions, $x = 0$ and $y = 0$, decreasing $\mathcal{K}$ by one with respect to the previous case. The solution of Eq. (2·7) for this orbit is $\kappa = 1$ and $\theta = \arcsin(\sqrt{\eta^2 - 1}/\eta)$. Its stationary point coincides with the separatrix values ($\sigma_1 = 1$, $\sigma_2 = 0$), corresponding formally to the caustic parameters ($u_c = \pi/2$, $v_c = 0$). (See the circle point with the vertical diameter in Fig. 1. In Fig. 1(b), this stationary point is very close to that for the elliptic orbits (3,1,1) in the meridian plane, which lies slightly on the right, along the $\sigma_2 = 0$ side.)

2.6. *Bifurcations*

At the deformations $\eta_{\rm bif}$ given by Eq. (2·8), the EQPO $M(n_v, n_\varphi)$ bifurcate, and the 3DPO or the hyperbolic 2DPO $M(n_v, n_\varphi, n_u)$ emerge. We encounter the breaking-of-symmetry problem at these bifurcation points, because the degeneracy (symmetry) parameter $\mathcal{K}$ changes there, for instance, from $\mathcal{K} = 1$ for the EQPO to $\mathcal{K} = 2$ for the 3DPO. Before the bifurcations ($\eta < \eta_{\rm bif}$), the stationary points σ_i of the 3DPO and the hyperbolic 2DPO are situated outside of the triangular tori region (2·5), and give rise to complex (κ, θ) and complex caustics. Such formal orbits are called "complex" or "ghost" orbits.[5] They cross the $\sigma_1 = \sigma_2$ boundary through the stationary points of the EQPO at bifurcations ($\eta = \eta_{\rm bif}$) and then move into the triangular tori region for larger η. In Fig. 1 are also indicated the stationary points for the 3DPO lying outside the physical tori region [(6,2,1) in Fig. 1(a), (7,2,1) and (8,2,1) in Fig. 1(b)]. The equatorial diameters $M(2, 1)$ correspond to the limiting case, $\sigma_1 = \sigma_2 = 0$. They bifurcate into themselves ($\mathcal{K} = 1$) and the hyperbolic 2DPO $(2M, M, 1)$ in the meridian plane ($\mathcal{K} = 2$) at the deformations given by Eq. (2·12).

The spherical limit ($\eta = 1$) is a special bifurcation point. In this limit, the planar regular polygons and diameters have degeneracies $\mathcal{K} = 3$ and 2, respectively, and they bifurcate into the meridian 2DPO ($\mathcal{K} = 2$), EQPO ($\mathcal{K} = 1$) and the isolated long diameter ($\mathcal{K} = 0$) for deformations $\eta > 1$.

The separatrix ($\sigma_1 = 1, \sigma_2 = 0$), related to the long diameter, is a special point in the phase space. Near this point, the complicated 3DPO and elliptic and hyperbolic 2DPO having large values of (n_u, n_v) and n_u/n_v close to 1/2 appear. Similar bifurcations of the 3DPO, EQPO and elliptic 2DPO appear near other boundary values of σ_i in the triangular tori on its "creeping" side $\sigma_1 = \sigma_1^+(\sigma_2)$, where some kinds of 3D "creeping" orbits with large values of n_v but finite and generally different n_u and n_φ appear. This is in analogy to the "creeping" singularities investigated for elliptic orbits in elliptic billiard systems[28] near the maximum value of σ_1, $\sigma_1^{\rm (cr)} = \cosh^2 v_b = \eta^2/(\eta^2 - 1)$, according to Eq. (A·6) at the right vertex in the "meridian-plane orbit" side $\sigma_2 = 0$. The 3DPO with a large number of the corners n_v and finite $n_u = n_\varphi$ approach the "creeping" elliptic orbits in the meridian plane. Another vertex corresponds to the creeping EQPO that have large values of n_v and n_φ but for $n_v/n_\varphi \to 1/2$.

The bifurcation point related to the appearance of "creeping" orbits cannot

be reached for any finite deformation. However, even for finite deformations like superdeformed shapes, the solutions for σ_1 and σ_2 [related to the roots κ and θ of the periodic-orbit conditions (2·7)] can be close to the "creeping" values of σ_1 and σ_2 [related to their boundary values given in (2·5)]. In such cases, we have to take into account such bifurcations in the trace formulas for the level density. The bifurcations of the 3D and 2D diameter-like orbits with n_v/n_u close to 1/2 near the separatrix are rather long, however, so that they are not important for the shell effects discussed below.

§3. Trace formulas for the prolate spheroid

3.1. *Phase-space trace formula in action-angle variables*

The level density $g(\varepsilon)$ is obtained from the Green function $G(\boldsymbol{r}, \boldsymbol{r}'; \varepsilon)$ by taking the imaginary part of its trace:

$$g(\varepsilon) = \sum_n \delta\left(\varepsilon - \varepsilon_n\right) = -\frac{1}{\pi} \operatorname{Im} \int d\boldsymbol{r}'' \int d\boldsymbol{r}' G(\boldsymbol{r}', \boldsymbol{r}''; \varepsilon)\ \delta(\boldsymbol{r}'' - \boldsymbol{r}'), \tag{3·1}$$

where ε_n is the single-particle energy. Following Ref. 28), we now apply the Gutzwiller trajectory expansion for the Green function $G(\boldsymbol{r}, \boldsymbol{r}', \varepsilon)$.[1),2),10)] After simple transformations,[28)] we obtain the phase-space trace formula in the action-angle variables $(\boldsymbol{I}, \boldsymbol{\Theta})$,

$$\begin{aligned} g_{\mathrm{scl}}(\varepsilon) = \frac{1}{(2\pi\hbar)^3} \operatorname{Re} \sum_\alpha \int d\boldsymbol{\Theta}'' \int d\boldsymbol{I}' \delta\left(\varepsilon - H\left(\boldsymbol{I}', \boldsymbol{\Theta}'\right)\right) \\ \times \exp\left[\frac{i}{\hbar}\left(S_\alpha\left(\boldsymbol{I}', \boldsymbol{I}'', t_\alpha\right) + \left(\boldsymbol{I}'' - \boldsymbol{I}'\right) \cdot \boldsymbol{\Theta}''\right) - i\frac{\pi}{2}\nu_\alpha\right], \end{aligned} \tag{3·2}$$

where the sum is taken over all classical trajectories α, $\boldsymbol{I} = \{I_u, I_v, I_\varphi\}$ represents the actions for the spheroidal cavity, $\boldsymbol{\Theta} = \{\Theta_u, \Theta_v, \Theta_\varphi\}$ the conjugate angles, and ν_α the phases related to the Maslov indices.[39),41)–43)] The phase-space trace formula (3·2) is especially useful for integrable systems, because the Hamiltonian H does not depend on the angle variables $\boldsymbol{\Theta}$ in this case, i.e., $H = H(\boldsymbol{I})$. The action

$$S_\alpha\left(\boldsymbol{I}', \boldsymbol{I}'', t_\alpha\right) = -\int_{\boldsymbol{I}'}^{\boldsymbol{I}''} d\boldsymbol{I} \cdot \boldsymbol{\Theta}(\boldsymbol{I}) \tag{3·3}$$

is related to the standard definition,

$$S_\alpha\left(\boldsymbol{\Theta}', \boldsymbol{\Theta}'', \varepsilon\right) = \int_{\boldsymbol{\Theta}'}^{\boldsymbol{\Theta}''} d\boldsymbol{\Theta} \cdot \boldsymbol{I}(\boldsymbol{\Theta}), \tag{3·4}$$

by the Legendre transformation

$$S_\alpha(\boldsymbol{\Theta}', \boldsymbol{\Theta}'', \varepsilon) + \boldsymbol{I}'' \cdot (\boldsymbol{\Theta}' - \boldsymbol{\Theta}'') = S_\alpha(\boldsymbol{I}', \boldsymbol{I}'', t_\alpha) + \boldsymbol{\Theta}'' \cdot (\boldsymbol{I}'' - \boldsymbol{I}'), \tag{3·5}$$

t_α being the time for a particle to revolve the trajectory α. The phase ν_α is specified below.

3.2. *Stationary phase method and classical degeneracy*

It should be emphasized that *even for integrable systems*, the trace integral (3·2) is more general than the Poisson-sum trace formula, which is the starting point of Refs. 5), 32) and 35) for the semiclassical derivations of the level density. These two trace formulas become identical when the phase of the exponent does not depend on the angle variables $\boldsymbol{\Theta}$. In this case, the integral over angles in (3·2) gives simply $(2\pi)^n$, where n is the dimension of the system ($n = 3$ for a spheroidal cavity), and the stationary condition for all angle variables are identities in the 2π interval. This is true for the *most degenerate* classical orbits, like the elliptic and hyperbolic 2DPO in the meridian plane and the 3DPO with $\mathcal{K} = n - 1 = 2$. However, for orbits with smaller degeneracies, like the EQPO ($\mathcal{K} = 1$) and the isolated long diameter ($\mathcal{K} = 0$), the exponent phase depends strongly on angles and possesses a definite stationary point. Therefore, we have to integrate over such angles using the ISPM in the same way as for the bifurcations of the isolated diameters in elliptic billiard systems.[28)]

3.3. *Stationary phase conditions*

Due to the appearance of the δ-function representing energy conservation, we can perform the integral over I'_v in Eq. (3·2) exactly, and the result is

$$g_{\rm scl}(\varepsilon) = \frac{1}{(2\pi\hbar)^3}\,{\rm Re}\sum_\alpha \int d\Theta''_u \int d\Theta''_v \int d\Theta''_\varphi \int dI'_u \int dI'_\varphi \frac{1}{|\omega'_v|} \times \exp\left[\frac{i}{\hbar}\left(S_\alpha\left(\boldsymbol{I}', \boldsymbol{I}'', t_\alpha\right) + \left(\boldsymbol{I}'' - \boldsymbol{I}'\right)\cdot\boldsymbol{\Theta}''\right) - i\frac{\pi}{2}\nu_\alpha\right]. \tag{3·6}$$

The integration limits for I_u and I_φ are determined by their relations to the variables (σ_1, σ_2) and by the boundaries given by Eq. (2·5). One of the trajectories, α_0, in the sum (3·6) is a special one that corresponds to the smooth level density $g_{\rm TF}$ of the Thomas-Fermi model.[10)] For all other trajectories, we first write the stationary phase conditions for the action variables I'_u and I'_φ as

$$\left(\frac{\partial S_\alpha(\boldsymbol{I}', \boldsymbol{I}'', t_\alpha)}{\partial I'_u}\right)^* - \Theta''_u \equiv \Theta'_u - \Theta''_u = 2\pi M_u, \tag{3·7a}$$

$$\left(\frac{\partial S_\alpha(\boldsymbol{I}', \boldsymbol{I}'', t_\alpha)}{\partial I'_\varphi}\right)^* - \Theta''_\varphi \equiv \Theta'_\varphi - \Theta''_\varphi = 2\pi M_\varphi, \tag{3·7b}$$

where $\boldsymbol{M} = (M_u, M_v, M_\varphi) = M(n_u, n_v, n_\varphi)$, and M is an integer which indicates the number of revolutions along the primitive periodic orbit β. The superscript asterisk indicates that we evaluate the quantities at the stationary point with $I'_u = I^*_u$ and $I'_\varphi = I^*_\varphi$. We next use the Legendre transformation (3·5). Then, the stationary phase conditions with respect to angles $(\Theta_u, \Theta_v, \Theta_\varphi)$ are given by

$$\left(\frac{\partial S_\alpha(\boldsymbol{\Theta}', \boldsymbol{\Theta}'', \varepsilon)}{\partial \boldsymbol{\Theta}''} + \frac{\partial S_\alpha(\boldsymbol{\Theta}', \boldsymbol{\Theta}'', \varepsilon)}{\partial \boldsymbol{\Theta}'}\right)^* \equiv \boldsymbol{I}'' - \boldsymbol{I}' = 0. \tag{3·8}$$

In the following derivations, we have to judge whether the stationary phase conditions (totally or partially) given by Eqs. (3·7) and (3·8) hold identically or only

at specific stationary points. For this purpose we have to calculate separately the contributions from the most degenerate 3DPO, the 2DPO families in the meridian plane ($\mathcal{K}=2$) and those from orbits with smaller degeneracies, like EQPO ($\mathcal{K}=1$) and the isolated long diameter ($\mathcal{K}=0$). The latter two kinds of orbits are different from the former two kinds with respect to the above-mentioned two possibilities concerning the integration over angles $\boldsymbol{\Theta}$.

3.4. *Three-dimensional orbits and meridian-plane orbits*

The most degenerate 3DPO and the meridian-plane (elliptic and hyperbolic) 2DPO with equal values of the action occupy some finite 3D areas between the corresponding caustic surfaces specified above. In this case, the stationary phase conditions (3·8) for the integration over all angle variables Θ_u, Θ_v and Θ_φ hold identically. The integrand does not depend on the angle variables, and the result of the integration is $(2\pi)^3$. Because Eq. (3·8) is identically satisfied [the action does not depend on the angles like the Hamiltonian $H(\boldsymbol{I})$] we have conservation of the action variables, $I'_u = I''_u = I_u$ and $I'_\varphi = I''_\varphi = I_\varphi$, along the classical trajectory α. The integrals over all Θ in Eq. (3·2) yield $(2\pi)^3$, and we are left with the Poisson-sum trace formula,[5),10)]

$$\begin{aligned} g_{\rm scl}(\varepsilon) &= \frac{1}{\hbar^3}\,{\rm Re}\sum_{\boldsymbol{M}}\int d\boldsymbol{I}\;\delta\left(\varepsilon - H(\boldsymbol{I})\right)\,\exp\left[\frac{2\pi i}{\hbar}\boldsymbol{M}\cdot\boldsymbol{I} - i\frac{\pi}{2}\nu_M\right] \\ &= \frac{1}{\hbar^3}\,{\rm Re}\sum_{\boldsymbol{M}}\int dI_u\int dI_\varphi\,\frac{1}{|\omega_v|}\,\exp\left[\frac{2\pi i}{\hbar}\boldsymbol{M}\cdot\boldsymbol{I} - i\frac{\pi}{2}\nu_M\right]. \end{aligned} \tag{3·9}$$

It is convenient to transform the integration variables (I_u, I_φ) into (σ_1, σ_2) defined by Eq. (2·3):

$$g_{\rm scl}(\varepsilon) = \frac{1}{\hbar^3}\,{\rm Re}\sum_{\boldsymbol{M}} p\zeta\int_{\sigma_2^-}^{\sigma_2^+}\frac{d\sigma_2}{2\sqrt{\sigma_2}}\int_{\sigma_1^-}^{\sigma_1^+} d\sigma_1\,\frac{\partial I_u}{\partial\sigma_1}\,\frac{1}{|\omega_v|}\,\exp\left[\frac{2\pi i}{\hbar}\,\boldsymbol{M}\cdot\boldsymbol{I} - i\frac{\pi}{2}\nu_M\right]. \tag{3·10}$$

The integration limits are greatly simplified when written in terms of $\sigma_i^\pm$ $(i=1,2)$ and form the triangular region shown in Fig. 1. We then integrate over σ_i, expanding the exponent phase about the stationary point $\sigma_i = \sigma_i^*$,

$$\begin{aligned} 2\pi\left(\boldsymbol{M}\cdot\boldsymbol{I}\right) &\equiv S_\alpha\left(\boldsymbol{I}, \boldsymbol{I}'', t_\alpha\right) + \left(\boldsymbol{I}''-\boldsymbol{I}\right)\cdot\boldsymbol{\Theta}'' \\ &= S_\beta(\varepsilon) + \frac{1}{2}\sum_{i,j} J_{ij}^\beta(\sigma_i-\sigma_i^*)(\sigma_j-\sigma_j^*) + \cdots, \end{aligned} \tag{3·11}$$

where $S_\beta(\varepsilon)$ is the action along the periodic orbit β,

$$S_\beta(\varepsilon) = 2\pi M\left[n_u I_u^* + n_v I_v\left(\varepsilon, I_u^*, I_\varphi^*\right) + n_\varphi I_\varphi^*\right], \tag{3·12}$$

and $I_v(\varepsilon, I_u, I_\varphi)$ is the solution of the energy conservation equation $\varepsilon = H(I_u, I_v, I_\varphi)$ with respect to I_v. Here, the single prime index is omitted for simplicity. The

quantity J_{ij}^{β} is the Jacobian stability factor with respect to σ_i along the energy surface,

$$J_{ij}^{\beta} = \left(\frac{\partial^2 S_\alpha}{\partial\sigma_i \partial\sigma_j}\right)_{\sigma_i=\sigma_i^*} = 2\pi M n_v K_{ij}^{\beta}, \tag{3·13}$$

and K_{ij}^{β} is the (2×2) curvature matrix of the energy surface evaluated at the stationary point $\sigma_i = \sigma_i^*$ (at the periodic orbit β):

$$K_{ij}^{\beta} = \frac{\partial^2 I_v}{\partial\sigma_i\partial\sigma_j} + \frac{\omega_u}{\omega_v}\frac{\partial^2 I_u}{\partial\sigma_i\partial\sigma_j} + \frac{\omega_\varphi}{\omega_v}\frac{\partial^2 I_\varphi}{\partial\sigma_i\partial\sigma_j}. \tag{3·14}$$

(See Appendix A for the explicit expressions of these curvatures.) As we see below, the off-diagonal curvature K_{12} is non-zero for variables σ_i.

Then we use the ISPM, where we keep exact finite limits for the integration over σ_i, and we finally obtain

$$\delta g^{(2)}_{\left\{{}^{\rm 3D}_{\rm 2D}\right\}}(\varepsilon) = \frac{1}{\varepsilon_0}\,{\rm Re}\sum_{\beta} A_{\beta}^{(2)}\,\exp\left(ikL_\beta - i\frac{\pi}{2}\nu_\beta\right), \tag{3·15}$$

where $\varepsilon_0 = \hbar^2/2mR^2$ ($R^3 = a^2 b$ due to the volume conservation condition). The sum runs over all two-parameter families of the 3DPO or the meridian-plane (elliptic and hyperbolic) 2DPO, and $A_{\beta}^{(2)}$ is the amplitude for a 3DPO or a 2DPO,*)

$$A^{(2)}_{\left\{{}^{\rm 3D}_{\rm 2D}\right\}} = \frac{1}{4\,\pi}\,\frac{L_\beta\zeta}{(Mn_vR)^2\sqrt{\sigma_2^*\,|\det K^\beta|}}\left[\frac{\partial I_u}{\partial\sigma_1}\right]_{\sigma_i=\sigma_i^*}\,{\rm erf}\left(\mathcal{Z}_1^-,\mathcal{Z}_1^+\right){\rm erf}\left(\mathcal{Z}_2^-,\mathcal{Z}_2^+\right). \tag{3·16}$$

Here, L_β represents "length" of the periodic orbit β,

$$\begin{aligned} L_\beta &= \frac{2\pi M n_v p}{m\omega_v} \\ &= 2Mn_v b\sin\theta\left[{\rm E}(\theta,\kappa) - \frac{{\rm F}(\theta,\kappa)}{{\rm F}\,(\kappa)}\,{\rm E}\,(\kappa) + \cot\theta\sqrt{1-\kappa^2\sin^2\theta}\right], \end{aligned} \tag{3·17}$$

where θ and κ are defined by the roots of the periodic-orbit equations (2·7) ($S_\beta = pL_\beta$ for cavities). This "length" taken at the stationary points σ_i^* [the real positive roots of Eq. (2·7) through Eqs. (2·4) and (2·6)] inside the finite integration range (2·5) represents the true length of the corresponding periodic orbit β. For other stationary points, the "length" is identical to the function (3·17) continued analytically outside the tori determined by (2·5). In Eq. (3·16) we also introduced the generalized error function ${\rm erf}\,(\mathcal{Z}^-,\mathcal{Z}^+)$ of the two complex arguments $\mathcal{Z}^-$ and $\mathcal{Z}^+$,

$${\rm erf}\left(z^-,z^+\right) = \frac{2}{\sqrt{\pi}}\int_{z^-}^{z^+} dz\,e^{-z^2} = {\rm erf}(z^+) - {\rm erf}(z^-), \tag{3·18}$$

*) The expression (3·16) is valid also for the 2DPO ($\sigma_2^* = 0$), because the product $\sigma_2 K_{22}$ is finite for any σ_2 (see Appendix A).

with $\mathrm{erf}(z)$ being the simple error function.[46] The arguments of these error functions are given by

$$\mathcal{Z}_1^{\beta\pm} = \sqrt{-i\pi M n_v K_{11}^\beta/\hbar}\left(\sigma_1^\pm(\sigma_2^*) - \sigma_1^*\right), \tag{3·19a}$$

$$\mathcal{Z}_2^{\beta\pm} = \sqrt{-i\pi M n_v (\det K^\beta/K_{11}^\beta)/\hbar}\left(\sigma_2^\pm - \sigma_2^*\right), \tag{3·19b}$$

in terms of the finite limits $\sigma_i^\pm$ given by (2·5), and taken at the stationary point $\sigma_2 = \sigma_2^*$. We note that, for the 3DPO $M(3t,t,1)$ with $t = 2,3,\cdots$, the curvature K_{11}^β is zero at any deformation. For such orbits, we should use

$$\mathcal{Z}_1^{\beta\pm} = \sqrt{-i\pi M n_v (\det K^\beta/K_{22}^\beta)/\hbar}\,\left(\sigma_1^\pm(\sigma_2^*) - \sigma_1^*\right), \tag{3·20a}$$

$$\mathcal{Z}_2^{\beta\pm} = \sqrt{-i\pi M n_v K_{22}^\beta/\hbar}\,\left[\sigma_2^\pm - \sigma_2^* + \frac{K_{12}^\beta}{K_{22}^\beta}\left(\sigma_1^\pm(\sigma_2^*) - \sigma_1^*\right)\right], \tag{3·20b}$$

in place of (3·19). The latter limits (3·20) are derived by changing the integration variable σ_2 to $\sigma_2 - (K_{12}/K_{22})(\sigma_1 - \sigma_1^*)$.

Let us consider the stationary points σ_i^* positioned far from the bifurcation points. This means that they are located far from the integration limits. Accordingly, the generalized error functions can be transformed into the complex Fresnel functions with real limits and then extend the upper limit to ∞ and the lower one to $-\infty$. In this way, we asymptotically obtain the Berry-Tabor result for the standard POT,[5] which is identical to the extended Gutzwiller result[9] for the most degenerate (3D and meridian-plane) orbit families,

$$A^{(2)}_{\left\{\begin{smallmatrix}\mathrm{3D}\\ \mathrm{2D}\end{smallmatrix}\right\}}(\varepsilon) = \frac{1}{\pi}\frac{L_\beta \zeta}{(M n_v R)^2\sqrt{\sigma_2^*|\det K^\beta|}}\left[\frac{\partial I_u}{\partial \sigma_1}\right]_{\sigma_i=\sigma_i^*}. \tag{3·21}$$

The constant part of the phase ν_β in Eq. (3·15), which is independent of η and ε, can be found by making use of the above asymptotic expression and applying the Maslov-Fedoryuk theory.[39),41)–43)] This theory relates the Maslov index μ_β with the number of turning and caustic points for the orbit family β. For the 3DPO, the total asymptotic phase ν_β is given by

$$\nu_{3\mathrm{D}} = \mu_{3\mathrm{D}} - \frac{1}{2}\epsilon_{3\mathrm{D}} + 2(Mn_u - 1), \quad \mu_{3\mathrm{D}} = M(3n_v + 2n_u). \tag{3·22}$$

Here, μ_β denotes the Maslov index, the numbers of caustic and turning points traversed by the orbit, and ϵ_β represents the difference of the numbers of positive and negative eigenvalues of curvature K^β.*) For the hyperbolic and elliptic meridian 2DPO, we obtain

$$\nu_{2\mathrm{DH}} = \mu_{2\mathrm{DH}} - \frac{1}{2}\epsilon_{2\mathrm{DH}} + 2\left(Mn_u - 1\right), \quad \mu_{2\mathrm{DH}} = 2M\left(n_v + n_u\right) \tag{3·23}$$

*) Because the dimension of K^β is 2, ϵ_β is written $\epsilon_\beta = \mathrm{sign}(K_1^\beta) + \mathrm{sign}(K_2^\beta)$, where K_i^β is the i-th eigenvalue of K^β. It can also be calculated by $\epsilon_\beta = \mathrm{sign}(K_{11}^\beta) + \mathrm{sign}(\det K^\beta/K_{11}^\beta)$ for $K_{11}^\beta \neq 0$, and $\epsilon_\beta = \mathrm{sign}(K_{22}^\beta) + \mathrm{sign}(\det K^\beta/K_{22}^\beta)$ for $K_{22}^\beta \neq 0$. Here, $\mathrm{sign}(x) = \pm 1$ for $x \gtrless 0$ and 0 for $x = 0$.

and

$$\nu_{\rm 2DE} = \mu_{\rm 2DE} - \frac{1}{2}\epsilon_{\rm 2DE} + 2\,(Mn_u - 1)\,, \quad \mu_{\rm 2DE} = 3Mn_v \tag{3·24}$$

respectively. Note that the total phase includes the argument of the complex amplitude (3·16), and it depends on both the deformation and energy.

Near the bifurcation deformations, the stationary points σ_i^* are close to the boundary of the finite area (2·5). In such cases, the asymptotic forms of the error functions are not good approximations, and we have to carry out the integration over σ_i in the calculation of the error functions in Eq. (3·16) exactly within the finite limits. It should also be noted that the contributions from "ghost" periodic orbits are important near the bifurcation points. They make the trace formula continuous as a function of η at all bifurcations.

Also when the stationary phase points σ_i^* are close to other boundaries of the tori, the integrals have to be evaluated with finite limits; for instance, near the triangular side $\sigma_1 = \sigma_1^+(\sigma_2)$, where we have the "creeping" points for the 3DPO inside the tori (2·5) and the meridian elliptic 2DPO near the endpoint ($\sigma_1 = \sigma_1^+$, $\sigma_2 = 0$) with a large number of vertices, $n_v \to \infty$. Another example of such a special bifurcation point is the separatrix ($\sigma_1 = 1$, $\sigma_2 = 0$), where 3DPO and hyperbolic 2DPO have a finite limit $n_u/n_v \to 1/2$ for $n_v \to \infty$ and $n_u \to \infty$. In this case, the curvature K_{11} becomes infinite, and the amplitude (3·16) approaches zero. Thus, to improve the trace formula near the bifurcations, we have to evaluate the generalized error integral $\mathrm{erf}(\mathcal{Z}_i^{\beta\,-}, \mathcal{Z}_i^{\beta\,+})$ (or corresponding complex Fresnel functions[46]) in Eq. (3·16) within the finite limits $\mathcal{Z}_i^{\beta\,\pm}$ given by Eq. (3·19) or (3·20).

For a spheroidal cavity, we have another bifurcation in the spherical limit, where the "azimuthal" Jacobian J_{22}^{β} and J_{12}^{β} (3·13) ($\sigma_2 \propto I_\varphi^2$) vanish.[9] This is the reason for the divergence of the standard POT result (3·21) in the spherical limit. Our improved trace formula (3·16) is finite in the spherical limit, because the "azimuthal" generalized error function $\mathrm{erf}(\mathcal{Z}_2^{\beta\,-}, \mathcal{Z}_2^{\beta\,+})$ is proportional to $\sqrt{J_{22}^{\beta}}$ in this limit, and thus this "azimuthal" Jacobian is exactly canceled by that coming from the denominator of Eq. (3·16). Thus, as shown in Ref. 9), the elliptic 2DPO term ($\mathcal{K}$=2) in the level density approaches the spherical Balian-Bloch result for the most degenerate planar orbits with larger degeneracy ($\mathcal{K} = 3$):

$$\delta g_{\rm sph}^{(3)}(\varepsilon) = \frac{\sqrt{kR}}{\varepsilon_0} \sum_{t\geq 1,\, q>2t} \sin\left(\frac{2\pi t}{q}\right) \sqrt{\frac{\sin(2\pi t/q)}{q\pi}} \times \sin\left[2kRq\sin\left(\frac{\pi t}{q}\right) - \frac{3\pi}{2}q - (t-1)\pi - \frac{\pi}{4}\right], \tag{3·25}$$

where $t = Mn_u$ and $q = Mn_v$. Note that Eq. (3·25) can be derived directly from the phase-space trace formula (3·2) or from the Poisson-sum trace formula, both rewritten in terms of the spherical action-angle variables.

3.5. *Equatorial-plane orbits*

We cannot apply the Poisson-sum trace formula (3·9) for equatorial-plane orbits, because, although the stationary-phase conditions for Θ_φ'' and Θ_v'' in Eq. (3·8) hold

identically, this is not the case for the angle variable Θ_u''. We thus apply the ISPM for the integration over Θ_u''.

Returning to Eq. (3·6), we transform the phase-space trace formula into new "parallel" $(\Theta_v''; I_v')$ and "perpendicular" $(\Theta_u'', \Theta_\varphi''; I_u', I_\varphi')$ variables, as explained in Appendix B for more general (integrable and non-integrable) systems. We then carry out the integration over the variables (I_u', I_φ') in terms of the ISPM by transforming them into the variables σ_i. Next, we consider the integration over the *angle* variable Θ_u'' using the ISPM, as there is an *isolated* stationary point at $\Theta_u^* = 0$ (or an integer multiple of 2π). We expand the exponent phase in a power series of Θ_u'' about $\Theta_u^* = 0$,

$$\begin{aligned} &S_\alpha\left(\boldsymbol{I}, \boldsymbol{I}'', t_\alpha\right) + \left(\boldsymbol{I}'' - \boldsymbol{I}\right) \cdot \boldsymbol{\Theta}'' \\ &\quad = pL_{\mathrm{EQ}} + \frac{1}{2}\sum_{ij} J_{ij}^{\mathrm{EQ}}(\sigma_i - \sigma_i^*)(\sigma_j - \sigma_j^*) + \frac{1}{2}J_\perp^{\mathrm{EQ}}\ \left(\Theta_u''\right)^2 + \cdots, \end{aligned} \tag{3·26}$$

where the stationary point $\sigma_1^* = \sigma_2^* \equiv \sigma^*$ is given by

$$\sigma^* = \left(\frac{I_\varphi^*}{p\zeta}\right)^2 = \frac{a^2\cos^2\phi}{\zeta^2} = \frac{\cos^2\phi}{\eta^2 - 1}, \qquad I_\varphi^* = p\,a\cos\phi. \tag{3·27}$$

The length of the equatorial polygon with n_v vertices and M rotations, L_{EQ}, is given by

$$L_{\mathrm{EQ}} = 2Mn_vR\sin\phi, \quad \phi = \pi n_\varphi/n_v. \tag{3·28}$$

In this way, we finally obtain the contribution of EQPO,

$$\delta g_{\mathrm{EQ}}^{(1)}(\varepsilon) = \frac{1}{\varepsilon_0}\,\mathrm{Re}\sum_{\mathrm{EQ}} A_{\mathrm{EQ}}^{(1)} \exp\left\{i\left(kL_{\mathrm{EQ}} - \frac{\pi}{2}\nu_{\mathrm{EQ}}\right)\right\}, \tag{3·29}$$

with the amplitudes $A_{\mathrm{EQ}}^{(1)}$ given by

$$A_{\mathrm{EQ}}^{(1)} = \sqrt{\frac{\sin^3\phi}{\pi Mn_vkR\eta F_z^{\mathrm{EQ}}}}\ \mathrm{erf}\left(\mathcal{Z}_1^-, \mathcal{Z}_1^+\right)\ \mathrm{erf}\left(\mathcal{Z}_2^-, \mathcal{Z}_2^+\right)\ \mathrm{erf}\left(\mathcal{Z}_3^-, \mathcal{Z}_3^+\right) \tag{3·30}$$

(see Appendix B for a detailed derivation). Here, $\mathcal{Z}_i^\pm$ are the limits given by Eq. (3·19) or (3·20) for $i = 1, 2$, and $\mathcal{Z}_3^- = 0, \mathcal{Z}_3^+ = \mathcal{Z}_\perp^+$ from Eq. (B·19). The latter is related to the finite limits $0 \le \Theta_u \le \pi/2$ for the angle Θ_u in the trace integration in Eq. (3·6), taking into account explicitly the factor 4, due to the time-reversal and spatial symmetries.

For the total asymptotic phase ν_{EQ}, we find

$$\nu_{\mathrm{EQ}} = \mu_{\mathrm{EQ}} + \frac{1}{2}, \quad \mu_{\mathrm{EQ}} = 3Mn_v, \tag{3·31}$$

where μ_{EQ} is the Maslov index. We calculated this phase using the Maslov-Fedoryuk theory[43] at a point asymptotically far from the bifurcations. Note that the total phase is defined as the sum of the asymptotic phase ν_{EQ} and the argument of the

Table I. Bifurcation points of some short periodic orbits.

periodic orbit	$\eta_{\rm bif}$	periodic orbit	$\eta_{\rm bif}$
(4,2,1)	$\sqrt{2}$	(6,3,1)	2
(5,2,1)	1.618...	(7,3,1)	2.247...
(6,2,1)	$\sqrt{3}$	(8,3,1)	2.414...
(7,2,1)	1.802...	(9,3,1)	2.532...
(8,2,1)	1.848...		

amplitude $A_{\rm EQ}$, given by Eq. (3·30), so that it depends on kR and η through the complex arguments of the product of the error functions. In the derivations of Eq. (3·30) we have taken into account the off-diagonal curvature, as in the previous subsection, but much smaller corrections due to the mixed derivatives of the action S_α with respect to Θ''_u and σ_i are ignored, taking $\sigma_i = \sigma_i^*$ in Eq. (3·26).

The bifurcation points are associated with zeros of the stability factor $F_z^{\rm EQ}$ and given by

$$\eta_{\rm bif} = \frac{\sin\phi}{\sin\left(n\phi/M\right)}, \qquad n = 1, 2, \cdots, M. \tag{3·32}$$

The bifurcation points most important for the superdeformed shell structure are listed in Table I.

When the stationary points are located inside the finite integration region far from the ends, we transform the error functions in Eq. (3·30) into the Fresnel functions and extend their arguments to $\pm\infty$, except in the case that the lower limit is exactly zero. From the definitions of the limit, Eqs. (3·19) and (B·19), for $\mathcal{Z}_i^{\pm}$, we have asymptotically $\mathcal{Z}_i^+ \to +\infty$ $(i = 1, 2, 3)$, $\mathcal{Z}_1^- = \mathcal{Z}_3^- \to 0$ and $\mathcal{Z}_2^- \to 0$ for diameters and $\mathcal{Z}_2^- \to -\infty$ for the other EQPO. Finally, we arrive at the standard Balian-Bloch formula[3] for the amplitude $A_{\rm EQ}^{(1)}$,

$$A_{\rm EQ}^{(1)} = \frac{f_{\rm EQ}}{\sqrt{\pi kR\eta}} \sqrt{\frac{\sin^3\phi}{Mn_v F_z^{\rm EQ}}}, \tag{3·33}$$

where $f_{\rm EQ} = 1$ for the diameters and 2 for the other EQPO [$\mathrm{erf}(\mathcal{Z}_2^-, \mathcal{Z}_2^+) \to f_{\rm EQ}$ in this limit].

As seen from Eq. (3·33), there is a divergence at the bifurcation points where $F_z^{\rm EQ} \to 0$. We emphasize that our ISPM trace formula (3·29) has no such divergences. Indeed, the stability factor $F_z^{\rm EQ}$ responsible for this divergence is canceled by $F_z^{\rm EQ}$ from the upper limit $\mathcal{Z}_3^+$, Eq. (B·19), of the last error function in Eq. (3·30), $\mathcal{Z}_3^+ \propto \sqrt{F_z^{\rm EQ}}$, and we obtain the following finite result at the bifurcation point:

$$A_{\rm EQ}^{(1)} = \frac{\eta^{1/3}\sin\phi\sqrt{\eta^2 - \sin^2\phi}}{\sqrt{2i(\eta^2-1)}Mn_v}\ \mathrm{erf}\left(\mathcal{Z}_1^-, \mathcal{Z}_1^+\right)\ \mathrm{erf}\left(\mathcal{Z}_2^-, \mathcal{Z}_2^+\right). \tag{3·34}$$

It is very important to note that there is a local enhancement of the amplitude

(3·34) by a factor of order $\sqrt{kR}$*) near the bifurcation point. This enhancement is associated with a change of the degeneracy parameter $\mathcal{K}$ by one locally near the bifurcation point. In general, any change of the degeneracy parameter $\mathcal{K}$ by $\Delta\mathcal{K}$ is accompanied by an amplitude enhancement by a factor of $(kR)^{\Delta\mathcal{K}/2}$, because $\Delta\mathcal{K}$ extra exact integrations are carried out. This enhancement mechanism of the amplitude obtained in the ISPM is quite general, and it is independent of the specific choice of the potential shapes.

We mention that a more general trace formula that can be applied also to non-integrable but axially symmetric systems can be derived from the phase-space trace formula (see Appendix B).

The contribution of the equatorial diameters in Eq. (3·29) for deformations far from bifurcation points reduces to the Balian-Bloch result for spherical diameters ($\mathcal{K} = 2$),

$$\delta g^{(2)}_{\rm sph}(\varepsilon) = -\frac{1}{\varepsilon_0}\sum_M \frac{1}{2\pi M}\,\sin(4MkR). \tag{3·35}$$

The amplitudes for planar polygons in the equatorial plane vanish in the spherical limit (see Appendix B). Note that the contributions of the planar polygons in the spherical cavity, Eq. (3·25), are obtained as the limit of $A^{(2)}_{\rm 2D}$, Eq. (3·16), for elliptic orbits in the meridian plane.[9)]

3.6. *Long diametric orbits and separatrices*

As mentioned in §2, the curvatures K^{β}_{ij} become infinite near the separatrix ($\sigma_1 = 1$, $\sigma_2 = 0$) (see Appendix C). This separatrix corresponds to the isolated long diameters ($\mathcal{K} = 0$) along the symmetry axis. Thus, for the derivation of their contributions to the trace formula, the expansion up to second order in action-angle variables considered above fails, as for the turning and caustic points in the usual phase space coordinates. However, we can apply the Maslov-Fedoryuk theory[39),41)–43)] in a similar way as the calculation of the Maslov indices associated with the turning and caustic points, but with the use of the action-angle variables in place of the usual phase-space variables. This is similar to the derivation of the long diametric term in the elliptic billiard.[28)]

Starting from the phase-space trace formula (3·6), we note that the spheroidal separatrix problem differs from that for the elliptic billiard system[28)] by the integrals over the two azimuthal variables Θ''_φ and I'_φ, which are additional to the integrals over Θ''_u and I'_u. We expand the phase of the exponent in Eq. (3·6) with respect to the action I'_φ and angle Θ''_φ about the stationary points $I^*_\varphi = 0$ and an arbitrary Θ^*_φ (for instance, $\Theta^*_\varphi = 0$), and take into account the *third* order terms, in a similar way as for the variables Θ''_u and I'_u (see Appendix C). Note that we consider here small deviations from the long diameters, and Θ^*_φ determines the azimuthal angle of the final point $\boldsymbol{r}''$ of this trajectory near the symmetry axis.

*) The parameter of our semiclassical expansion is in practice $\sqrt{kL_\beta}\left(\propto\sqrt{kR}\right)$. It is actually large for 3D orbits ($L_\beta \sim 10R$) associated with superdeformed shell structures in nuclei.

After the procedure explained in Appendix C, we obtain

$$\delta g^{(0)}_{\rm LD}(\varepsilon) = \frac{\pi b}{2\varepsilon_0 R}\,{\rm Re}\sum_M \frac{1}{kR}\, e^{ikL_{\rm LD}-i\frac{\pi}{2}\nu_{\rm LD}} \prod_{j=1}^{2} e^{\frac{2i}{3}\left[(w_j^{\parallel})^{3/2}+(w_j^{\perp})^{3/2}\right]} \frac{\left(w_j^{\parallel}w_j^{\perp}\right)^{1/4}}{\sqrt{|c_{2,j}^{\parallel}c_{2,j}^{\perp}|}}$$
$$\times[{\rm Ai}(-w_j^{\parallel}) + i\,{\rm Gi}(-w_j^{\parallel})]$$
$$\times[{\rm Ai}(-w_j^{\perp},\mathcal{Z}_{\perp}^{-},\mathcal{Z}_{\perp}^{+}) + i\,{\rm Gi}(-w_j^{\perp},\mathcal{Z}_{\perp}^{-},\mathcal{Z}_{\perp}^{+})] \tag{3·36}$$

(see Appendix C for the notation used here).

For finite deformations and sufficiently large kR, i.e. for large $p\zeta \propto kR\sqrt{\eta^2-1}$, near the separatrix $\sigma_1 \to 1, \sigma_2 \to 0$, the incomplete Airy functions in this equation can be approximated by the complete ones. Thus, Eq. (3·36) reduces to the standard Gutzwiller result for isolated diameters,[3),9)]

$$\delta g^{(0)}_{\rm LD}(\varepsilon) = \frac{2b}{\pi\varepsilon_0 kR^2}\sum_M \frac{1}{|F^{\rm LD}_{xy}|}\cos\left[kL_{\rm LD}(M) - \frac{\pi}{2}\nu_{\rm LD}\right], \tag{3·37}$$

with the length $L_{\rm LD}(M) = 4Mb = 4M\eta^{2/3}R$ and the stability factor $F^{\rm LD}_{xy}$ for long diameters given by Eq. (C·20).

For the calculation of the asymptotic phase $\nu_{\rm LD}$, we use this asymptotic expression and calculate the Maslov indices $\mu_{\rm LD}$ using the Maslov-Fedoryuk theory,[43)] obtaining

$$\nu_{\rm LD} = \mu_{\rm LD} + 2, \quad \mu_{\rm LD} = 4M. \tag{3·38}$$

The additional phases, dependent on deformation and energy, come from the arguments of the complex exponents and Airy functions of the complex amplitude.

In the spherical limit, both the upper and lower limits of the incomplete Airy functions in Eq. (3·36) approach zero, and the angle integration has the finite limit $\pi/2$ (see Appendix C). With this, the other factors ensure that the amplitude for long diameters becomes zero; that is, the long diametric contribution to the level density vanishes in the spherical limit.

§4. Level density, shell energy and averaging

4.1. *Total level density*

In spheroidal cavity systems, the ISPM total semiclassical level density can be written as a sum over all periodic orbit families:

$$\delta g_{\rm scl}(\varepsilon) = \delta g^{(2)}_{\rm 3D}(\varepsilon) + \delta g^{(2)}_{\rm 2D}(\varepsilon) + \delta g^{(1)}_{\rm EQ}(\varepsilon) + \delta g^{(0)}_{\rm LD}(\varepsilon) = \sum_{\beta}\delta g^{(\beta)}_{\rm scl}(\varepsilon), \tag{4·1}$$

where the first two terms represent the contributions from the most degenerate ($\mathcal{K} = 2$) families of periodic orbits, the 3DPO and the meridian-plane 2DPO, given by Eq. (3·15), the third term the EQPO given by Eq. (3·29), and the fourth term the long diameters given by Eq. (3·36).

4.2. *Semiclassical shell energy*

The shell energy δE can be expressed in terms of the oscillating part $\delta g_{\rm scl}^{(\beta)}(\varepsilon)$ of the semiclassical level density (4·1) as[4),9),10)]

$$\delta E = \sum_{\beta} \left(\frac{\hbar}{t_\beta}\right)^2 \delta g_{\rm scl}^{(\beta)}(\varepsilon_{\rm F}), \qquad N = \int_0^{\varepsilon_{\rm F}} d\varepsilon\, g(\varepsilon). \tag{4·2}$$

Here, t_β denotes the period for a particle moving with the Fermi energy $\varepsilon_{\rm F}$ along the periodic orbit β,

$$t_\beta = MT_\beta = \frac{2\pi M}{\Omega_\beta}, \tag{4·3}$$

T_β being the primitive period ($M = 1$), M the number of repetitions, and Ω_β the frequency. The Fermi energy $\varepsilon_{\rm F}$ is determined by the second equation of (4·2), where N is the particle number.

In the derivation of Eq. (4·2) we used an expansion of the amplitudes $A_\beta(\varepsilon)$ about the Fermi energy $\varepsilon = \varepsilon_{\rm F}$. Although the $A_\beta(\varepsilon)$ are oscillating functions of the energy ε (or kR), we can apply such an expansion, because the A_β are much smoother than the oscillations coming from the exponent function of kL_β. The latter oscillations are responsible for the shell structure, while the oscillations of A_β merely lead to slight modulations with much smaller frequencies.

Thus, the trace formula for δE differs from that for δg only by the factor $(\hbar/t_\beta)^2 = (\hbar^2 k_{\rm F}/mL_\beta)^2$ near the Fermi surface, i.e. longer orbits are additionally suppressed by the factor $1/L_\beta^2$. The semiclassical shell energy is therefore determined by short periodic orbits.

4.3. *Average level density*

For the purpose of presentation of the level density improved at the bifurcations we need to consider only an average level density, thus also avoiding the convergence problems that usually arise when one is interested in a full semiclassical quantization.

The average level density is obtained by folding the level density with a Gaussian of width Γ:

$$g_\Gamma(\varepsilon) = \frac{1}{\sqrt{\pi}\Gamma} \int_{-\infty}^{\infty} d\varepsilon'\, g(\varepsilon')\, e^{-(\frac{\varepsilon-\varepsilon'}{\Gamma})^2}. \tag{4·4}$$

The choice of the Gaussian form of the averaging function is insignificant and is made here only for the sake of mathematical simplicity.

Applying now the averaging procedure defined above to the semiclassical level density (4·1), we obtain[3),9)]

$$\delta g_{\Gamma,{\rm scl}}(\varepsilon) = \sum_{\beta} \delta g_{\rm scl}^{(\beta)}(\varepsilon)\, e^{-(\frac{\Gamma MT_\beta}{2\hbar})^2} = \sum_{\beta} \delta g_{\rm scl}^{(\beta)}(\varepsilon)\, e^{-(\frac{\gamma L_\beta}{2R})^2}. \tag{4·5}$$

The latter equation is written specifically for cavity problems in terms of the orbit length L_β (in units of the typical length scale R) and the dimensionless parameter γ defined by

$$\Gamma = 2\gamma\sqrt{\varepsilon\varepsilon_0}\ , \tag{4·6}$$

where γ is the averaging width with respect to kR. Thus, the averaging yields an exponential decrease of the amplitudes with increasing L_β and γ. In Ref. 9), the value of γ is chosen to be 0.6. In this case, all longer orbits are strongly damped and only the short periodic orbits contribute to the oscillating part of the level density. For the study of the bifurcation phenomena in the superdeformed region, we need a significantly smaller value of γ.

Finally, we can say that the contribution of an orbit family to the average density of states is more important as the degeneracy of the orbit is higher, and as the volume occupied by the orbit family in the phase space is larger, and also as the length of the orbit is shorter.

§5. Quantum spheroidal cavity

5.1. *Oscillating level density*

We calculated the quantum spectrum using the spherical wave decomposition method,[50] in which wave functions are decomposed into the spherical waves as

$$\psi_m(\boldsymbol{r}) = {\sum_l}' C_l\, j_l(kr)\, Y_{lm}(\Omega). \tag{5·1}$$

Here, m denotes the magnetic quantum number, and $\sum'$ indicates that l is summed over even (odd) numbers for positive (negative) parity states. The functions j_l and Y_{lm} are the usual spherical Bessel functions and spherical harmonics, respectively. The expansion coefficients C_l are determined so that the wave function (5·1) satisfies the Dirichlet boundary condition

$$\psi_m(r = R(\Omega)) = 0, \tag{5·2}$$

or equivalently,

$$\int d\Omega Y^*_{lm}(\Omega)\psi_m(r = R(\Omega)) = 0, \quad {}^\forall l. \tag{5·3}$$

By inserting (5·1) into (5·3), we obtain the matrix equation

$${\sum_{l'}}' B_{ll'}(k)C_{l'} = 0, \quad B_{ll'}(k) = \int d\Omega Y^*_{lm}(\Omega) j_{l'}(kR(\Omega))Y_{l'm}(\Omega). \tag{5·4}$$

Truncating the summation l at a sufficiently large number l_c, we can obtain the energy eigenvalue $\varepsilon_n = \hbar^2 k_n^2/2m$ by searching for the roots satisfying

$$\det B(k_n) = 0. \tag{5·5}$$

Figure 5 displays the energy level diagram for the prolate spheroidal cavity as functions of the axis ratio $\eta > 1$. In Fig. 6, we plot shell structure energy

$$\delta E(N, \eta) = \sum_{n=1}^{N} \varepsilon_n(\eta) - \tilde{E}(N, \eta) \tag{5·6}$$

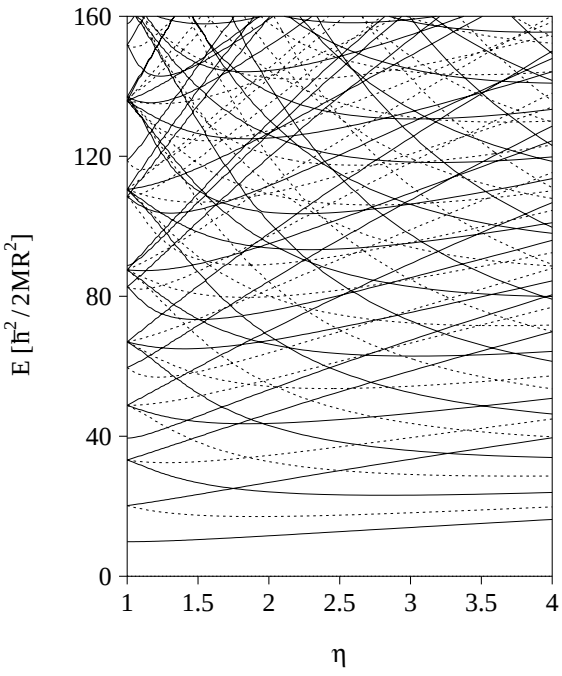

Fig. 5. Single-particle spectrum for the spheroidal cavity as a function of the axis ratio η. Solid and dashed curves represent the positive and negative parity levels, respectively.

as a function of η and particle number N. As well as the strong shell effect at the spherical shape ($\eta = 1$), one clearly sees a prominent shell structure for a superdeformed shape ($\eta \sim 2$).

Next, we calculated the coarse-grained level density with the usual Strutinsky smoothing procedure by treating the wave number k as smoothing variable:

$$g_\gamma(k) = \frac{1}{\gamma}\int_0^\infty dk' R\, f_M\left(\frac{kR - k'R}{\gamma}\right) g(k'). \tag{5·7}$$

As the smoothing function $f_M(x)$, we use a Gaussian with M-th order curvature corrections,

$$f_M(x) = \frac{1}{\sqrt{\pi}} e^{-x^2} L_{M/2}^{1/2}(x^2), \tag{5·8}$$

where $L_n^\alpha(z)$ represents a Laguerre polynomial. Equation (4·4) corresponds to the case of $M = 0$. In the following, we set the order of curvature corrections to $M = 6$ and the smoothing width to $\tilde{\gamma} = 2.5$, with which we can nicely satisfy the plateau condition.[44] A coarse-graining is also performed using the same smoothing function but with smaller γ. We define the oscillating part of the level density by subtracting the smooth part as

$$\delta g_\gamma(k) = g_\gamma(k) - g_{\tilde{\gamma}}(k). \tag{5·9}$$

The left-hand side of Fig. 7 displays $\delta g_\gamma(k)$ with $\gamma = 0.3$ as a function of η and

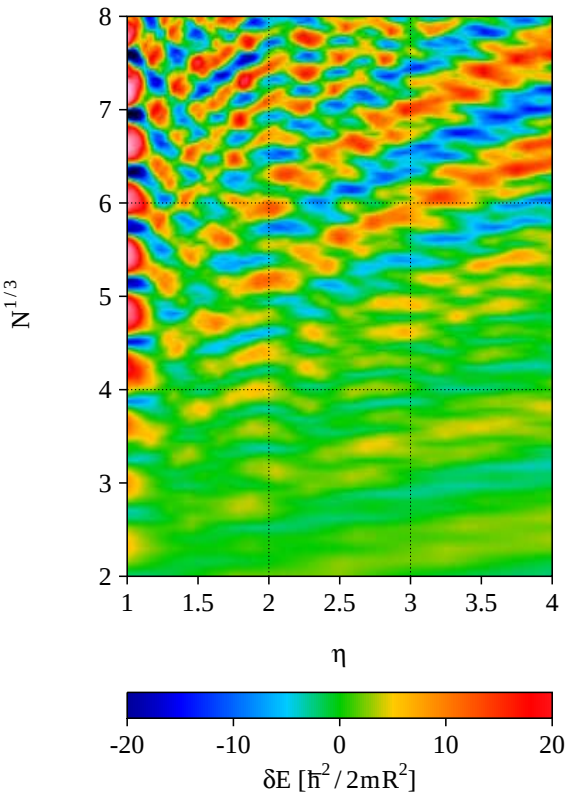

Fig. 6. Shell structure energy δE as a function of η and $N^{1/3}$, where N is the neutron (proton) number, taking the spin-degeneracy factor into account. Energies are counted in units of $\hbar^2/2mR^2$ ($\sim 30A^{-2/3}$MeV).

kR. It is seen that a clear shell structure emerges for $\eta \sim 2$, corresponding to the superdeformed shape.

Let us consider the mechanism of this strong shell effect. If a single orbit makes a dominant contribution to the periodic-orbit sum

$$\delta g_{\rm scl}(\varepsilon) = \sum_{\beta} a_\beta(k)\cos(kL_\beta - \pi\nu_\beta/2), \quad a_\beta(k) = A_\beta/\varepsilon_0, \tag{5·10}$$

the major oscillating pattern in δg should be determined by the phase factor of the dominant term. In that case, the positions of the valley curves for δg in the (η, kR) plane are given by

$$kL_\beta - \pi\nu_\beta/2 = (2n+1)\pi. \qquad (n = 0, 1, 2, \cdots) \tag{5·11}$$

The right-hand side of Fig. 7 plots the *stationary action curves* (5·11) for several periodic orbits. The green solid curves represent the triangular orbit in the meridian plane. The other longer meridian orbits exhibit the same behavior but with smaller distances. The red dashed curves represent the star-shaped orbit with five vertices in

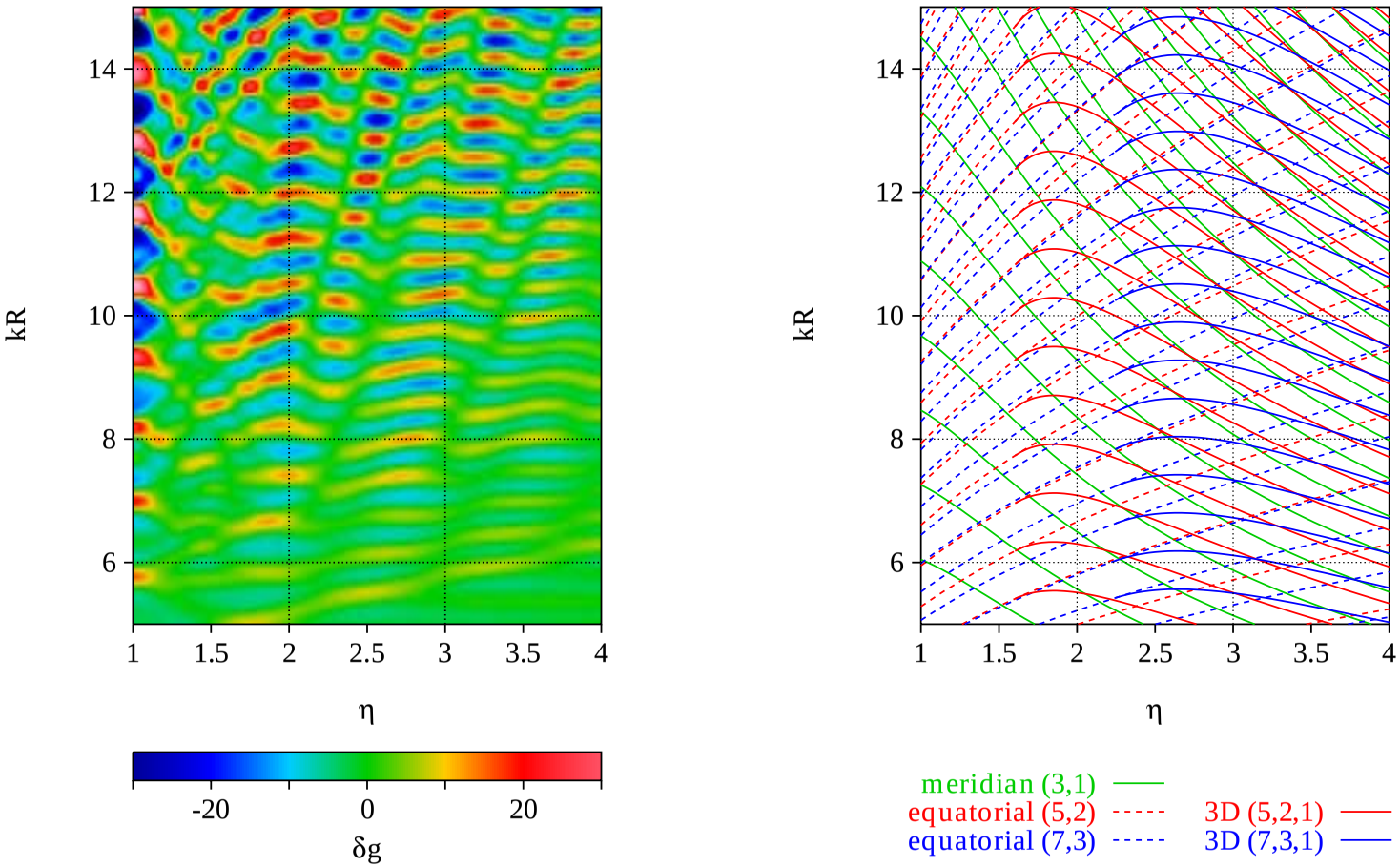

Fig. 7. Oscillating part δg of the single-particle level density as a function of η and kR (left-hand side) and stationary-action curves for several periodic orbits (right-hand side). A clear correspondence between the enhancement of the shell effect and the periodic-orbit bifurcations is seen.

the equatorial plane. It bifurcates at $\eta = 1.618\ldots$ and the 3D orbit (5,2,1) thereby appears (red solid curves). The sequence $(n, 2, 1)$ $(n = 5, 6, 7, \cdots)$ exhibit similar behaviors, shifting the bifurcation points slightly to larger η. Comparing with the plot of quantum δg, there is a clear correspondence between the superdeformed shell structure and the bifurcation of above star-shaped orbits. There is also a correspondence between the bifurcations of the equatorial-plane orbits $(n, 3)$ $(n = 7, 8, 9, \cdots)$ with the hyperdeformed shell structure emerging at $\eta \simeq 2.5$. The significant shell energy gain occurring at the superdeformed shape obtained in Fig. 6 is considered to be a result of this strong shell effect in the level density.

5.2. *Fourier analysis of the level density*

Fourier analysis is a useful tool to investigate the quantum-classical correspondence in the level density.[3)] Due to the simple form of the action integral $S_\beta = \hbar k L_\beta$, it is easy to Fourier transform the semiclassical level density $g_{\rm scl}(k)$ with respect to k. Let us define the Fourier transform $F(L)$ by

$$F(L) = \int dk e^{-ikL} g(k). \tag{5·12}$$

In actual numerical calculations, we multiply the integrand of the right-hand side of this equation by a Gaussian truncation function, obtaining

$$F_\Delta(L) = \frac{\Delta}{\sqrt{2\pi}} \int dk e^{-\frac{1}{2}(k\Delta)^2} e^{-ikL} g(k). \tag{5·13}$$

Inserting the semiclassical level density (5·10), the Fourier transform is expressed as

$$F_\Delta^{\rm scl}(L) = \bar{F}_\Delta(L) + \frac{1}{2} \sum_\beta e^{-i\pi\nu_\beta/2} a_\beta \left(i \frac{\partial}{\partial L} \right) \exp\left[-\frac{1}{2} \left(\frac{L - L_\beta}{\Delta} \right)^2 \right]. \tag{5·14}$$

This is a function that has peaks at the lengths of the classical periodic orbits $L = L_\beta$. On the other hand, we can calculate $F(L)$ by inserting the quantum mechanical level density $g(k) = \sum_n \delta(k - k_n)$ as

$$F_\Delta^{\rm qm}(L) = \frac{\Delta}{\sqrt{2\pi}} \sum_n e^{-\frac{1}{2}(k_n\Delta)^2} e^{-ik_n L}. \tag{5·15}$$

This quantity should exhibit successive peaks at orbit lengths $L = L_\beta$. Thus we can extract information concerning classical periodic orbits from the quantum spectrum. On the left-hand side of Fig. 8, we plot the Fourier transform (5·15) as a function of L and η. On the right-hand side of Fig. 8, the lengths of classical periodic orbits $L_\beta(\eta)$ are shown. There, red curves represent the orbits $M(n_v, 2, 1)$ $(n_v = 4, 5, 6, \cdots)$. We find strong Fourier peaks at $\eta \simeq 2$, corresponding to the periodic orbits (5,2,1), (6,2,1) and (7,2,1) just after the bifurcation points. We also find Fourier peaks at $\eta \simeq 2.5$, corresponding to the periodic orbits (7,3,1) and (8,3,1), etc. Thus, we can conclude that these periodic orbit bifurcations play essential roles in the emergence of superdeformed and hyperdeformed shell structures.

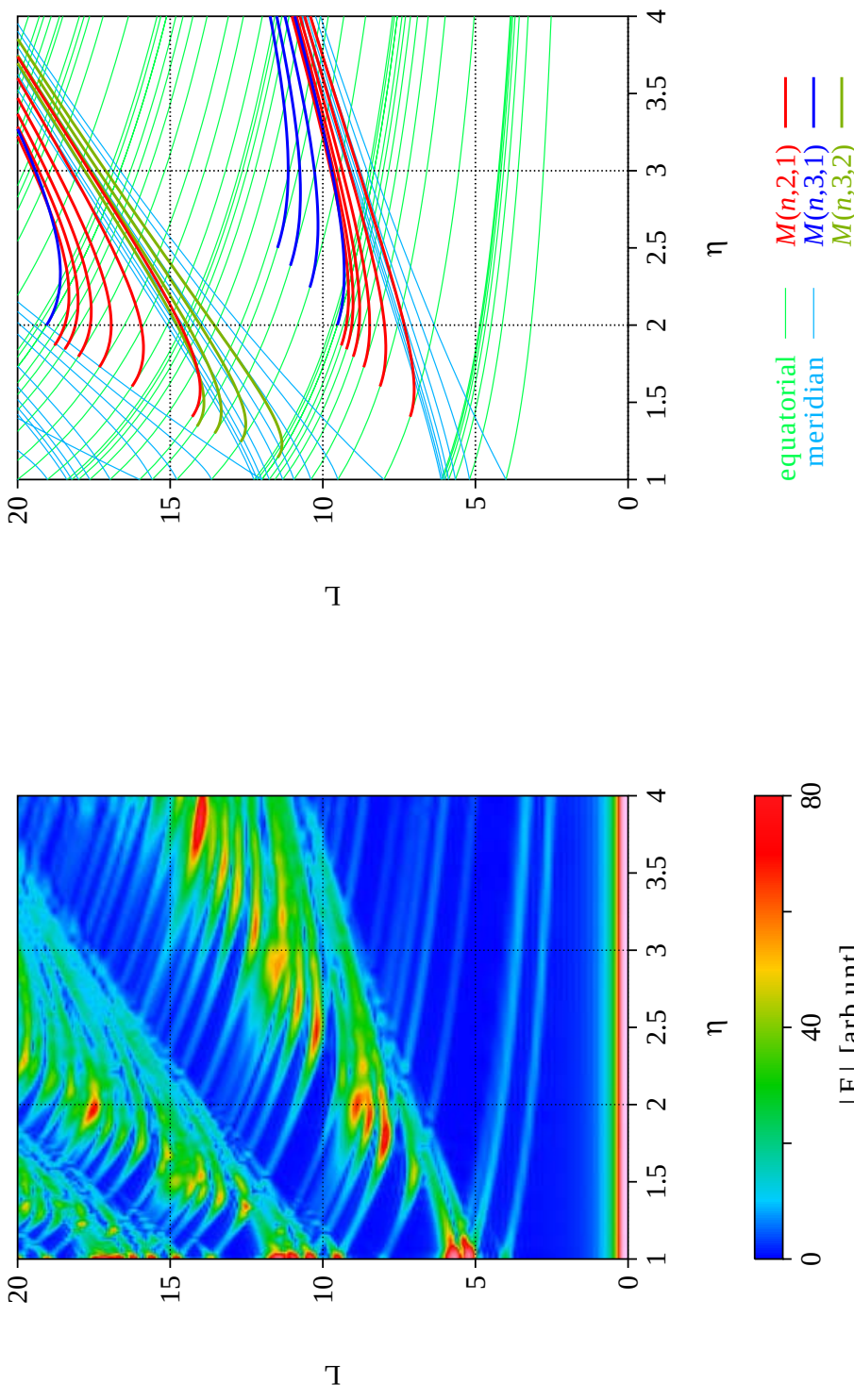

Fig. 8. Fourier amplitude $|F(L)|$ of the single-particle level density (left-hand side) and lengths of classical periodic orbits (right-hand side).

5.3. *Coarse-grained shell structure energy*

In order to prove that the shell structure at the superdeformed shape is due to the bifurcated orbits, we calculated the 'coarse-grained' shell energy defined by

$$\delta\tilde{E}_\gamma(N) = \int^{\tilde{k}_{\rm F}(\gamma)} \varepsilon(k) g_\gamma(k) dk - \int^{\tilde{k}_{\rm F}(\tilde{\gamma})} \varepsilon(k) g_{\tilde{\gamma}}(k) dk, \tag{5·16}$$

where the smoothed Fermi wave number $\tilde{k}_{\rm F}$ in each term is determined so that they satisfy the particle number condition

$$\int^{\tilde{k}_{\rm F}(\gamma)} g_\gamma(k) dk = \int^{\tilde{k}_{\rm F}(\tilde{\gamma})} g_{\tilde{\gamma}}(k) dk = N. \tag{5·17}$$

By coarse-graining with the width γ, a shell structure of resolution $\Delta kR = \gamma$ is extracted. Classical orbits relevant to such a structure are those with lengths

$$L < L_{\rm max} = \frac{2\pi R}{\gamma}. \tag{5·18}$$

Setting $\gamma = 0.6$, contributions from periodic orbits with $L \gtrsim 10R$ are smeared out. Around the superdeformed shape, bifurcated orbits have lengths $L \sim 10R$, and these contributions are significantly weakened by smoothing with $\gamma = 0.6$, and the major oscillating pattern of δE should disappear if these bifurcated orbits are responsible

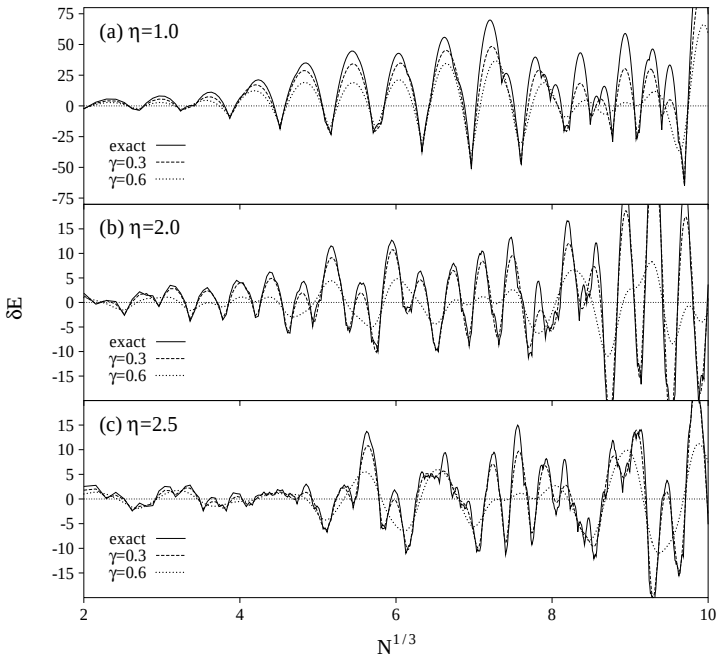

Fig. 9. Shell structure energies plotted as functions of $N^{1/3}$. Solid curves represent the exact shell structure energies. Dashed and dotted curves represent those calculated by using the coarse-grained level density $g_\gamma(k)$ with the smoothing widths $\gamma = 0.3$ and 0.6, respectively.

for the superdeformed shell effect. In Fig. 9, the coarse-grained shell energies (5·16) calculated for $\eta = 1, 2$ and 2.5 with $\gamma = 0.3$ and 0.6 are compared with the exact shell structure energies. In the upper panel, it is seen that the spherical shell structure survives after smoothing with $\gamma = 0.6$, indicating that the major structure is determined by orbits whose lengths are sufficiently shorter than $10R$. In contrast with it, the middle panel shows that the major oscillating pattern of the superdeformed shell structure is considerably broken after smoothing with $\gamma = 0.6$. The same argument is valid also for $\eta = 2.5$. This strongly supports the significance of bifurcated orbits for the superdeformed and hyperdeformed shell structures.

§6. Enhancement of semiclassical amplitudes near the bifurcation points

In this section, we present some results of the semiclassical ISPM calculation, which clearly show enhancement phenomena of the semiclassical amplitudes $|A_{3D}|$ and $|A_{EQ}|$ near the bifurcation points.

Figure 10(a) shows the modulus of the complex amplitude A_{3D} [Eq. (3·16)]

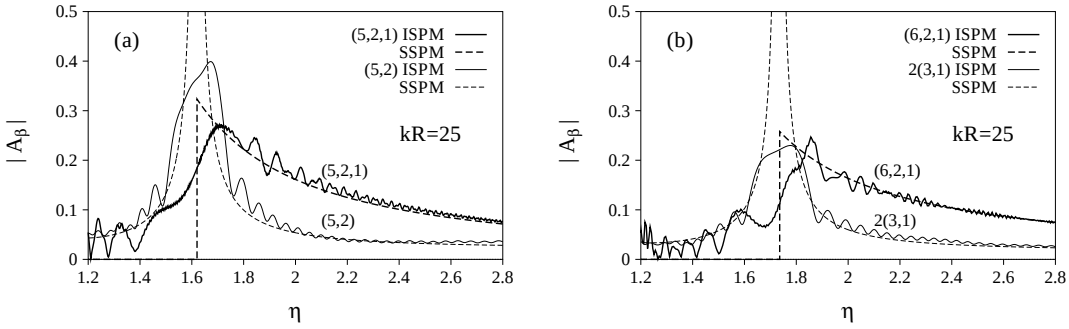

Fig. 10. (a) Semiclassical amplitudes $|A_{3D}|$ for the 3DPO (5,2,1) and $|A_{EQ}|$ for the EQPO (5,2), calculated at $kR = 25$ with the ISPM, are plotted as functions of the deformation parameter η by thick and thin solid curves, respectively. They are compared with the SSPM amplitudes (dashed curves). (b) The same as (a), but for the 3DPO (6,2,1) and the EQPO 2(3,1).

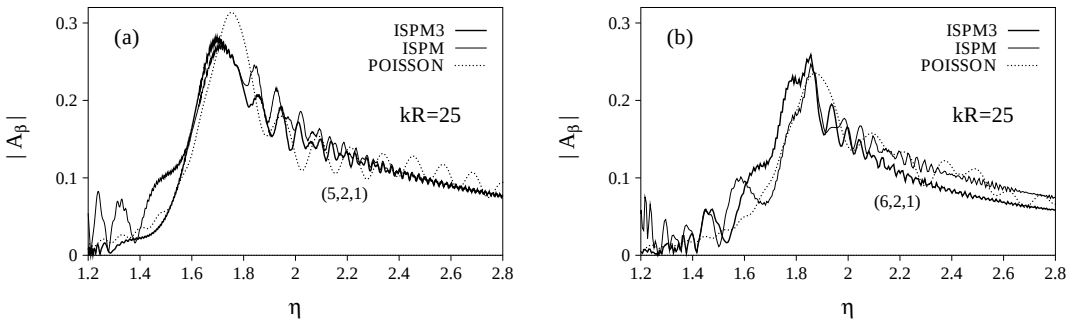

Fig. 11. (a) ISPM3 amplitudes for the 3DPO (5,2,1), calculated at $kR = 25$, are plotted as functions of the deformation η by thick-solid curves. For comparison, the ISPM amplitudes and the results of exact integration in the Poisson-sum trace formula are plotted by thin-solid and thick-dotted curves, respectively. (b) The same as (a), but for the 3DPO (6,2,1).

for the 3DPO $(5,2,1)$ and $A_{\rm EQ}$ [Eq. (3·30)] for the EQPO $(5,2)$ as functions of the deformation parameter η. They are compared with those of the SSPM. The SSPM amplitude for the EQPO $(5,2)$ is divergent at the bifurcation deformation $\eta_{\rm bif} = 1.618\ldots$, while the ISPM amplitude is finite and continuous through this bifurcation point, with a rather sharp maximum at this point. This difference is due to a local change of the symmetry parameter $\mathcal{K}$ from 1 to 2 at the bifurcation, and the associated enhancement of the amplitude is of order $\sqrt{kR}$. As seen from Fig. 10(a), the ISPM amplitude for the $(5,2,1)$ is continuous through the bifurcation point and exhibits a significant enhancement slightly to the right of it. It approaches the SSPM amplitude given by Eq. (3·21) away from the bifurcation point. The ISPM enhancement for the 3DPO is also of order $\sqrt{kR}$, because here, as in the case of the bifurcating EQPO, the degeneracy parameter $\mathcal{K}$ changes from 1 to 2. The same is true for the 3DPO (6,2,1) and the EQPO 2(3,1), as shown in Fig. 10(b).

In Fig. 11, we consider corrections from the 3rd-order terms in the expansion of the action about the stationary point. Here we incorporate the 3rd-order terms in the variable σ_1 (ISPM3) which are expected to be important for the 3DPO (6,2,1) whose curvature K_{11} is identically zero (see Appendix D). We also show results of the exact integration in the Poisson-sum trace formula (3·10) (marked "POISSON"). It is seen that the results of the ISPM3 for the $(5,2,1)$ and $(6,2,1)$ orbits are in good agreement with those of the ISPM in the most important regions, near the bifurcations, and on their right-hand sides. It is gratifying to see that the ISPM and the ISPM3 amplitudes $|A_{\rm 3D}|$ for $(5,2,1)$ and $(6,2,1)$ are also in good agreement with the results of the exact integration in the Poisson-sum trace formula. With the 3rd-order corrections, excessive ghost orbit contributions in the ISPM (bumps in the ISPM amplitudes on the left-hand side of the bifurcation point) are removed, and better agreement with the result of the exact integration is obtained. Except for this, the corrections due to the 3rd-order terms are rather small, and good convergence is achieved up to the second-order terms.

The amplitudes $|A_\beta|$ are slightly oscillating functions of kR. Because the period of this oscillation is much larger than that of the shell energy oscillation, the expansion about the Fermi energy $\varepsilon_{\rm F}$ (or $k_{\rm F}R$) can be used in the derivations of both the semiclassical ISPM shell energy $\delta E_{\rm scl}$ and the oscillating level density $\delta g_{\rm scl}$ (3·15). Figure 12 displays the semiclassical amplitudes $A_{\rm 3D}$ for the 3DPO (5,2,1) and $A_{\rm EQ}$ for the EQPO $(5,2)$ as functions of kR at $\eta = 1.618\ldots$ (top panel) and $\eta = 2$ (bottom panel). In this figure, the semiclassical amplitudes $A_{\rm 3D}$ for the 3DPO (6,2,1) and $A_{\rm EQ}$ for the EQPO 2(3,1) are also plotted as functions of kR at the bifurcation point $\eta = \sqrt{3}$ (middle panel). We see that for $\eta = 2$ the amplitudes $|A_{\rm 3D}|$ for the 3DPO $(5,2,1)$ and $(6,2,1)$ become much larger than the amplitude $|A_{\rm EQ}|$ for the EQPO.

§7. Comparison between quantum and semiclassical calculations

In this section we present results of calculations of the level densities and shell energies using the quantum Strutinsky method and the semiclassical ISPM, and make comparisons between the quantum and semiclassical calculations. In the quantum

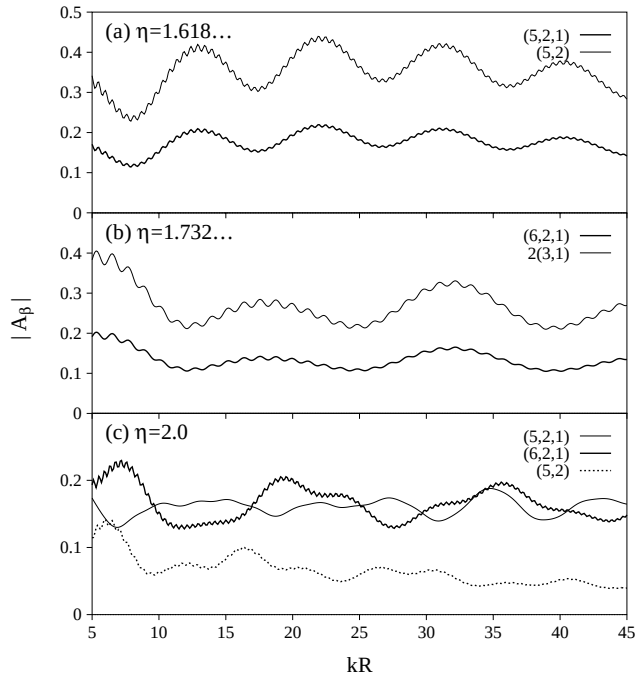

Fig. 12. (a) Semiclassical amplitudes $|A_{3D}|$ for the 3DPO (5,2,1) and $|A_{EQ}|$ for the EQPO (5,2) plotted by bold and thin solid curves, respectively, as functions of kR at the bifurcation point $\eta = 1.618\ldots$. (b) The same as (a), but for the 3DPO (6,2,1) and the EQPO 2(3,1) at the bifurcation point $\eta = 1.732\ldots$. (c) Semiclassical amplitudes $|A_{3D}|$ for (5,2,1), (6,2,1) and $|A_{EQ}|$ for (5,2) plotted by thin-solid, thick-solid and dotted curves, respectively, as functions of kR at $\eta = 2.0$.

calculations, the averaging parameter $\gamma = 0.3$ is used.

Figure 13 displays oscillating level densities δg for relatively small deformations. There, QM and ISPM denote the δg obtained with the quantum Strutinsky method and the semiclassical ISPM, respectively. For $\eta = 1.2$ we obtain good convergence of the periodic orbit sum (4·1) by taking into account the short elliptic 2DPO with $n_v \leq 12$, $n_u = 1$, the short EQPO with the maximum vertex number $p_{\max} = M(n_v)_{\max} = 14$, and the maximum winding number $t_{\max} = Mn_\varphi = 1$ ($M = 1, n_\varphi = 1$). The ISPM result is in good agreement with the quantum result. For the bifurcation point $\eta = \sqrt{2}$ of the butterfly orbit $(4, 2, 1)$ and $\eta = 1.5$ slightly to the right of it, the convergence of the periodic-orbit sum is achieved by taking into account the contributions from the bifurcating orbits, $(4, 2, 1)$ and the twice-repeated diameter $2(2, 1)$ with $t_{\max} = 2$, in addition to the 2DPO and the EQPO considered in the $\eta = 1.2$ case.

Figure 14 presents the oscillating level densities for the bifurcation deformations: $\eta = 1.618\ldots$ for the EQPO $(5, 2)$, $\eta = \sqrt{3}$ for the EQPO $2(3, 1)$, and $\eta = 2$ for the triply repeated equatorial diameters $3(2, 1)$. It is interesting to compare this figure with Fig. 15, where some results of simplified semiclassical calculations are given. In the top panel of Fig. 15, the SSPM is used instead of the ISPM. We see that the

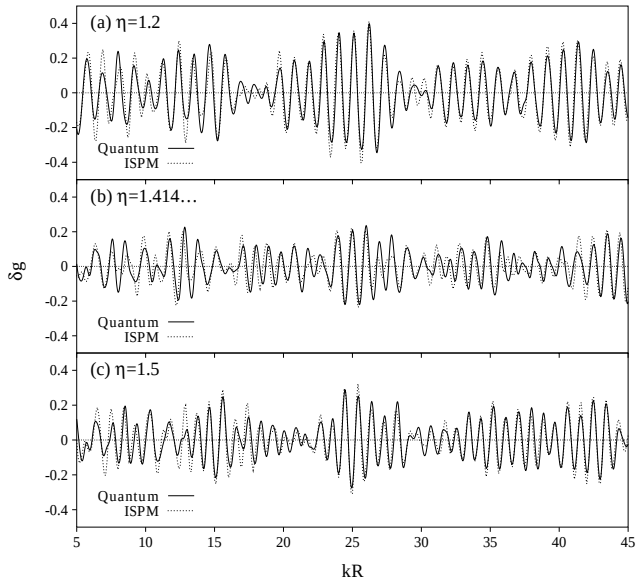

Fig. 13. Oscillating level densities evaluated with the semiclassical ISPM and a quantum mechanical method are shown by dotted and solid curves, respectively, as functions of kR for several deformations η.

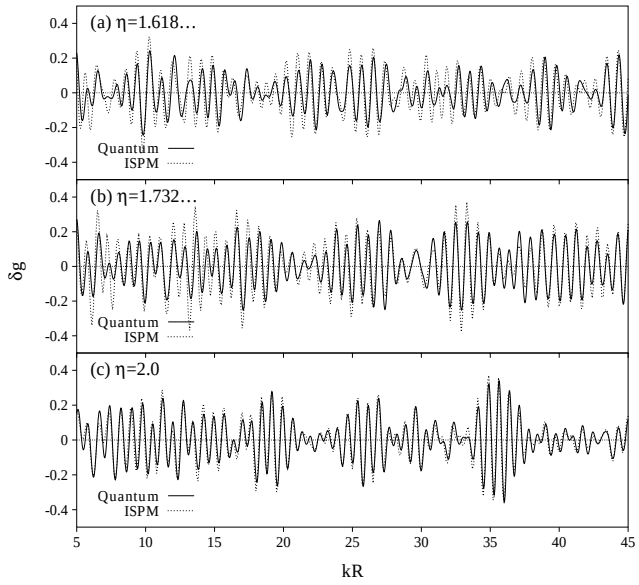

Fig. 14. The same as Fig. 13 but for larger deformations.

SSPM is a good approximation for $\eta = 1.2$. In the middle and bottom panels, only bifurcating orbits are taken into account in the periodic-orbit sum: Only the 3DPO $(5, 2, 1)$, the EQPO $(5, 2)$ and the butterfly $(4, 2, 1)$ are accounted for in the middle panel, while only the 3DPO $(5, 2, 1)$, $(6, 2, 1)$, $(7, 2, 1)$ and $(8, 2, 1)$ in the bottom panel. By comparing with the corresponding ISPM results shown in Fig. 15, we see

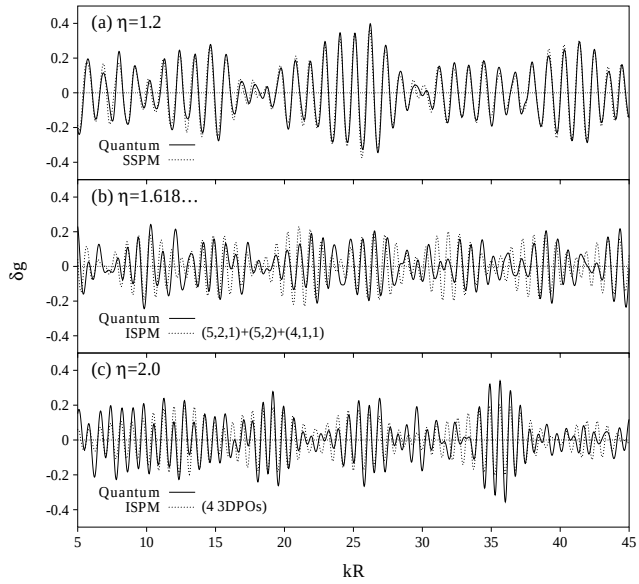

Fig. 15. Comparison of the oscillating level densities calculated with a quantum mechanical method (solid curves) and those obtained with some specific semiclassical calculations (dotted curves): (a) the top panel gives a comparison with the SSPM result for $\eta = 1.2$; (b) the middle panel displays the ISPM result in which only the bifurcating 3DPO $(5, 2, 1)$, the EQPO $(5, 2)$ and the 2DPO butterfly $(4, 2, 1)$ are taken into account for the POT sum in Eq. (3·15) for $\eta = 1.618\ldots$; (c) the bottom panel displays the ISPM result, in which only the four shortest 3DPO are taken into account for $\eta = 2.0$.

that, for $\eta = 1.618\ldots$ and 2, the major patterns of the oscillation are determined by these short 3DPO.

Figures 16 and 17 display the shell energies, which respectively correspond to the oscillating level densities shown in Figs. 13 and 14. Again, we see good agreement between the results of the semiclassical ISPM and the quantum calculations. For $\eta = 1.2$, good convergence is obtained by including only the shortest elliptic 2DPO and EQPO, in the same way as for the level density δg (see Ref. 9)). For $\eta = \sqrt{2}$ and 1.5, the properties of the ISPM shell energies are similar to those considered for the elliptic billiard system in Ref. 28). Now, let us more closely examine the bifurcation effects in the superdeformed region by comparing Fig. 17 with Fig. 18. In the top panel of Fig. 18, we show the ISPM result for $\eta = 1.618\ldots$ in which only the bifurcating 3DPO $(5, 2, 1)$, the short EQPO $(5, 2)$ and the hyperbolic 2DPO $(4, 2, 1)$ are taken into account. In the middle panel of this figure, we show the ISPM shell energies at $\eta = 1.732\ldots$, calculated by taking into account only the 3DPO $(5, 2, 1)$, the bifurcating 3DPO $(6, 2, 1)$ and the EQPO $2(3, 1)$. These comparisons clearly indicate that a few dominant periodic orbits determine the properties of the quantum shell structure at those bifurcation deformations. The bottom panel in this figure displays the dominant contributions of only the few shortest 3DPO at $\eta = 2.0$. Evidently, the short 3DPO $(5, 2, 1)$, $(6, 2, 1)$, $(7, 2, 1)$ and $(8, 2, 1)$ determine the major oscillating pattern of the shell energy. Thus, we can say that they are

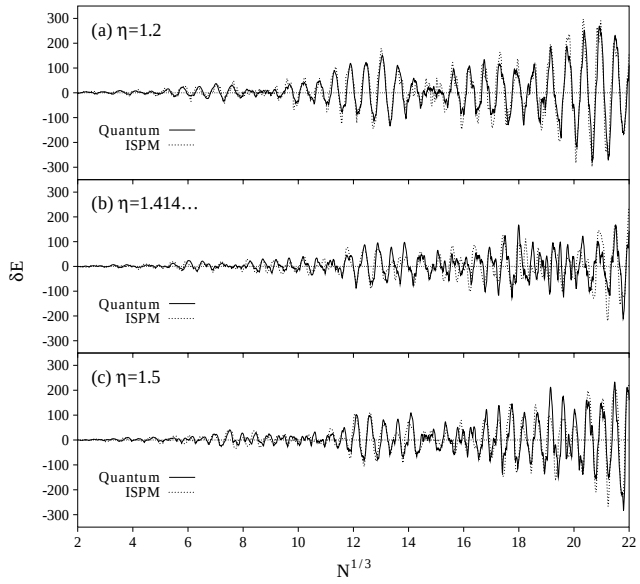

Fig. 16. Semiclassical ISPM and quantum shell energies (in units of ε_0) are plotted by dotted and solid curves, respectively, as functions of $N^{1/3}$.

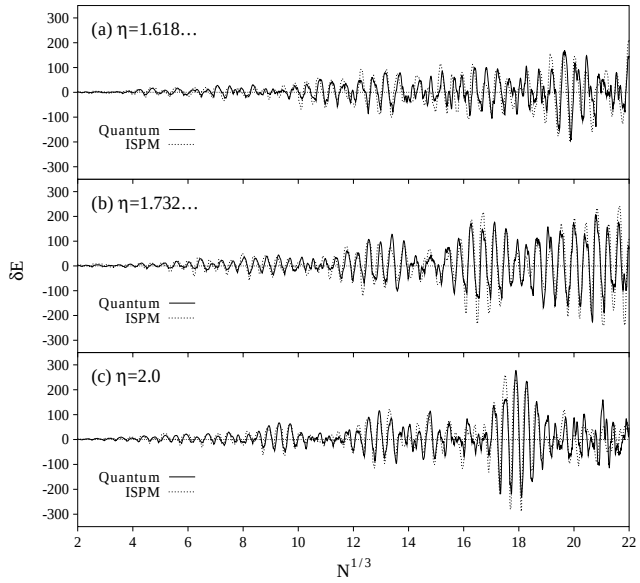

Fig. 17. The same as Fig. 16, but for larger deformations.

responsible for the formation of the shell structure at large deformations around the superdeformed shape. These results of the calculation are in good agreement with those obtained in Ref. 23) from the analysis of the length spectra (Fourier transforms of the quantum level densities).

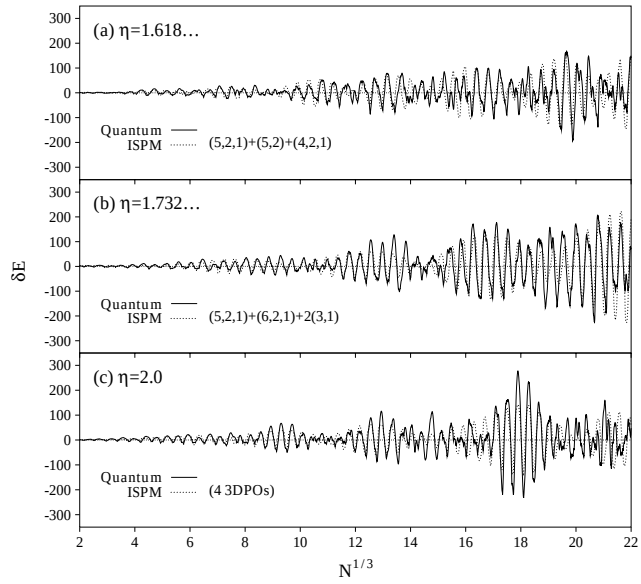

Fig. 18. Comparison of quantum shell energies (solid curves) with those obtained with specific semiclassical calculations (dotted curves): (a) the top panel presents the ISPM result for $\eta = 1.618...$, where only the bifurcating orbits (5,2,1), (5,2) and (4,2,1) are taken into account; (b) the middle panel displays for $\eta = 1.732...$ the contributions of *only* three orbits, the 3DPO $(5, 2, 1)$ and $(6, 2, 1)$, and the EQPO $2(3, 1)$; (c) the bottom panel plots for $\eta = 2.0$ the contributions of *only* the four shortest 3DPO to the ISPM sum.

§8. Conclusion

We have obtained an analytical trace formula for the 3D spheroidal cavity model, which is continuous through all critical deformations where bifurcations of periodic orbits occur. We find an enhancement of the amplitudes $|A_\beta|$ at deformations $\eta \sim 1.6$–2.0 due to bifurcations of 3D orbits from the short 2D orbits in the equatorial plane. The cause of this enhancement is quite general and independent of the specific potential shapes. We believe that this is an important mechanism that contributes to the stability of superdeformed systems, also in the formation of the second minimum related to the isometric states in nuclear fission. Our semiclassical analysis may therefore lead to a deeper understanding of shell structure effects in superdeformed fermionic systems — not only in nuclei and metallic clusters, but also, e.g., in deformed semiconductor quantum dots whose conductance and magnetic susceptibilities are significantly modified by shell effects.

Acknowledgements

A.G.M. gratefully acknowledges the financial support provided under the COE Professorship Program by the Ministry of Education, Science, Sports and Culture of Japan (Monbu-sho), giving him the opportunity to work at the RCNP and thanks

Prof. H. Toki for his warm hospitality and fruitful discussions. We acknowledge valuable discussions with Prof. M. Brack. Two of us (A.G.M. and S.N.F.) thank also the Regensburger Universitätsstiftung Hans Vielberth and Deutsche Forschungsgemeinshaft (DFG) for financial support.

Appendix A
— *Curvatures* —

A.1. *Three-dimensional orbits*

The action is written

$$S = 2\pi M \left(n_v I_v + n_u I_u + n_\varphi I_\varphi\right), \tag{A·1}$$

where I_u, I_v and I_φ are the partial actions. In a dimensionless form, they are

$$I_u = \frac{p\zeta}{\pi}\tilde{I}_u, \qquad I_v = \frac{p\zeta}{\pi}\tilde{I}_v, \qquad I_\varphi = \frac{p\zeta}{\pi}\tilde{I}_\varphi, \tag{A·2}$$

where

$$\tilde{I}_u = 2\int_0^{z_-} \frac{dz}{1-z^2}\sqrt{(z^2-z_-^2)(z^2-z_+^2)}, \tag{A·3a}$$

$$\tilde{I}_v = \int_{z_+}^{z_b} \frac{dz}{z^2-1}\sqrt{(z^2-z_-^2)(z^2-z_+^2)}, \tag{A·3b}$$

$$\tilde{I}_\varphi = \pi\sqrt{\sigma_2}. \tag{A·3c}$$

The quantities $z_\pm$ are related to the variables σ_i by

$$z_+^2 + z_-^2 = \sigma_1 + 1, \qquad z_+^2 z_-^2 = \sigma_1 - \sigma_2. \tag{A·4}$$

In terms of the elliptic integrals, (A·3) can be expressed as

$$\tilde{I}_u = \frac{2}{z_+}\left[(z_-^2-1)\mathrm{F}(k) - \sigma_2\Pi(z_-^2,k) + z_+^2\mathrm{E}(k)\right], \tag{A·5a}$$

$$\tilde{I}_v = \frac{1}{z_+}\left\{(z_+^2-z_-^2)\left[\mathrm{F}(\varphi,k) - \Pi(\varphi,n,k)\right] - z_+^2\mathrm{E}(\varphi,k)\right\} + z_b\sin\varphi, \tag{A·5b}$$

with

$$k = \frac{z_-}{z_+}, \quad n = \frac{1-z_-^2}{1-z_+^2}, \quad \varphi = \arcsin\sqrt{\frac{z_b^2-z_+^2}{z_b^2-z_-^2}}, \quad z_b = \cosh v_b = \frac{\eta}{\sqrt{\eta^2-1}}. \tag{A·6}$$

Here, we have used the standard definitions of the elliptic integrals of the first and the third kind,*)

$$\mathrm{F}(\varphi,k) = \int_0^\varphi \frac{dx}{\sqrt{1-k^2\sin^2 x}}, \tag{A·7a}$$

*) The definitions of the elliptic integrals (A·7) are related with those in Ref. 46) as $\mathrm{F}(\theta,\kappa) \equiv \mathrm{F}(\theta|\alpha)$ and $\Pi(\theta,n,\kappa) = \Pi(n,\theta|\alpha)$ $(\kappa = \sin\alpha)$.

$$\mathrm{E}(\varphi,k)=\int_0^{\varphi}\sqrt{1-k^2\sin^2 x}\,dx, \tag{A·7b}$$

$$\Pi(\varphi,n,k)=\int_0^{\varphi}\frac{dx}{(1-n\sin^2 x)\sqrt{1-k^2\sin^2 x}}, \tag{A·7c}$$

and we have omitted the argument $\varphi=\pi/2$ for complete elliptic integrals.

The action (A·1) is written as

$$S=2p\zeta M\left(n_v\tilde{I}_v+n_u\tilde{I}_u+n_\varphi\tilde{I}_\varphi\right). \tag{A·8}$$

The curvatures K_{ij} of the energy surface $\varepsilon=H(\sigma_1,\sigma_2,\varepsilon)$ are defined as

$$K_{ij}=\frac{p\zeta}{\pi}\tilde{K}_{ij}=\frac{\partial^2 I_v}{\partial\sigma_i\partial\sigma_j}+\frac{\omega_u}{\omega_v}\frac{\partial^2 I_u}{\partial\sigma_i\partial\sigma_j}+\frac{\omega_\varphi}{\omega_v}\frac{\partial^2 I_\varphi}{\partial\sigma_i\partial\sigma_j}, \tag{A·9}$$

and the frequency ratios in Eq. (A·9) are given by

$$\frac{\omega_u}{\omega_v}\equiv-\left(\frac{\partial I_v}{\partial I_u}\right)_{I_\varphi}=-\frac{\partial\tilde{I}_v/\partial\sigma_1}{\partial\tilde{I}_u/\partial\sigma_1}, \tag{A·10}$$

$$\frac{\omega_\varphi}{\omega_v}\equiv-\left(\frac{\partial I_v}{\partial I_\varphi}\right)_{I_u}=-\frac{2\sqrt{\sigma_2}}{\pi}\left[\frac{\partial\tilde{I}_v}{\partial\sigma_2}+\frac{\omega_u}{\omega_v}\frac{\partial\tilde{I}_u}{\partial\sigma_2}\right]. \tag{A·11}$$

We have used here the properties of Jacobians for the transformations from the variables (I_u,I_φ) to (σ_1,σ_2). For the first derivatives of the actions (A·3) with respect to σ_1 and σ_2, we obtain

$$\frac{\partial\tilde{I}_u}{\partial\sigma_1}=\frac{1}{z_+}\mathrm{F}(k),\qquad \frac{\partial\tilde{I}_v}{\partial\sigma_1}=-\frac{1}{2z_+}\mathrm{F}(\varphi,k), \tag{A·12a}$$

$$\frac{\partial\tilde{I}_u}{\partial\sigma_2}=-\frac{1}{z_+}\Pi(z_-^2,k),\quad \frac{\partial\tilde{I}_v}{\partial\sigma_2}=C_{\mathrm{F}}\,\mathrm{F}(\varphi,k)+C_\Pi\,\Pi(\varphi,n,k), \tag{A·12b}$$

with

$$C_{\mathrm{F}}=\frac{z_+^2-1}{2z_+\sigma_2}=-\frac{1}{2z_+(z_-^2-1)},$$
$$C_\Pi=-\frac{z_+^2-z_-^2}{2z_+\sigma_2}=\frac{z_+^2-z_-^2}{2z_+(z_+^2-1)(z_-^2-1)}. \tag{A·13}$$

For the second derivatives of these actions, we obtain

$$\frac{\partial^2\tilde{I}_u}{\partial\sigma_1^2}=\frac{1}{2z_+^3}\left\{\frac{1}{k^2}\left[\Pi(k^2,k)-\mathrm{F}(k)\right]\left(\frac{\partial z_-^2}{\partial\sigma_1}-k^2\frac{\partial z_+^2}{\partial\sigma_1}\right)-\frac{\partial z_+^2}{\partial\sigma_1}\mathrm{F}(k)\right\}, \tag{A·14a}$$

$$\frac{\partial^2\tilde{I}_v}{\partial\sigma_1^2}=-\frac{1}{4z_+^3}\left\{\frac{1}{k^2}\left[\Pi(\varphi,k^2,k)-\mathrm{F}(\varphi,k)\right]\left(\frac{\partial z_-^2}{\partial\sigma_1}-k^2\frac{\partial z_+^2}{\partial\sigma_1}\right)\right.$$
$$\left.-\frac{\partial z_+^2}{\partial\sigma_1}\mathrm{F}(\varphi,k)+\frac{2z_+^2}{\Delta_\varphi}\frac{\partial\varphi}{\partial\sigma_1}\right\}, \tag{A·14b}$$

$$\frac{\partial^2 \tilde{I}_u}{\partial \sigma_2^2} = \frac{1}{2z_+^5 k_1^2}\left[\Pi(z_-^2,k) + 2z_+^2\,\frac{\partial \Pi(z_-^2,k)}{\partial n} + \frac{1+k^2}{k}\,\frac{\partial \Pi(z_-^2,k)}{\partial k}\right], \tag{A·14c}$$

$$\frac{\partial^2 \tilde{I}_v}{\partial \sigma_2^2} = \frac{\partial C_{\rm F}}{\partial \sigma_2}\,{\rm F}(\varphi,k) + C_{\rm F}\left(\frac{1}{\Delta_\varphi}\frac{\partial \varphi}{\partial \sigma_2} + \frac{\partial {\rm F}(\varphi,k)}{\partial k}\frac{\partial k}{\partial \sigma_2}\right) + \frac{\partial C_\Pi}{\partial \sigma_2}\,\Pi(\varphi,n,k)$$
$$+C_\Pi\left(\frac{\partial \Pi(\varphi,n,k)}{\partial \varphi}\frac{\partial \varphi}{\partial \sigma_2} + \frac{\partial \Pi(\varphi,n,k)}{\partial n}\frac{\partial n}{\partial \sigma_2} + \frac{\partial \Pi(\varphi,n,k)}{\partial k}\frac{\partial k}{\partial \sigma_2}\right), \tag{A·14d}$$

and

$$\frac{\partial^2 \tilde{I}_u}{\partial \sigma_1 \partial \sigma_2} = -\frac{1}{2z_+^5 k_1^2}\left[{\rm F}(k) + \frac{1+k^2}{k}\,\frac{\partial {\rm F}(k)}{\partial k}\right], \tag{A·14e}$$

$$\frac{\partial^2 \tilde{I}_v}{\partial \sigma_1 \partial \sigma_2} = \frac{1}{4z_+^5 k_1^2}\left[{\rm F}\,(\varphi,k) - \frac{(\sigma_1+1-2z_b^2)\tan\theta}{\Delta_\varphi z_b^2 \Delta_\theta^2 k_1} + \frac{1+k^2}{k}\,\frac{\partial {\rm F}(\varphi,k)}{\partial k}\right]. \tag{A·14f}$$

Here,

$$\Delta_x = \sqrt{1-k^2\sin^2 x}, \quad k_1 = \sqrt{1-k^2}, \quad \theta = \arcsin\left(\frac{z_+}{z_b}\right), \tag{A·15}$$

and

$$\frac{\partial z_\pm^2}{\partial \sigma_1} = \frac{1}{2}\left[1 \pm \frac{\sigma_1 - 1}{\sqrt{(\sigma_1-1)^2+4\sigma_2}}\right] = \frac{1}{2}\left[1 \pm \frac{z_+^2+z_-^2-2}{z_+^2-z_-^2}\right], \tag{A·16}$$

$$\frac{\partial \varphi}{\partial \sigma_1} = \frac{1}{2}\,\frac{\frac{\partial z_-^2}{\partial \sigma_1}(z_b^2-z_+^2) - \frac{\partial z_+^2}{\partial \sigma_1}(z_b^2-z_-^2)}{(z_b^2-z_-^2)\sqrt{(z_b^2-z_+^2)(z_+^2-z_-^2)}}, \tag{A·17}$$

$$\frac{\partial k^2}{\partial \sigma_2} = -\frac{1+k^2}{z_+^4 k_1^2}, \tag{A·18}$$

$$\frac{\partial C_{\rm F}}{\partial \sigma_2} = \frac{z_-^2 - 2z_+^2 - 1}{4z_+^3(1-z_-^2)^2(z_+^2-z_-^2)}, \tag{A·19}$$

$$\frac{\partial C_\Pi}{\partial \sigma_2} = -\frac{\sigma_2(3z_+^2+z_-^2) - 2z_+^2(z_+^2-z_-^2)^2}{4z_+^3\sigma_2^2(z_+^2-z_-^2)}, \tag{A·20}$$

$$\frac{\partial \varphi}{\partial \sigma_2} = \frac{\left(2z_b^2 - (\sigma_1+1)\right)\tan\theta}{2z_b^2 z_+^4 k_1^3 \Delta_\theta^2}, \tag{A·21}$$

$$\frac{\partial n}{\partial \sigma_2} = \frac{\sigma_1 - 1}{(1-z_+^2)^2(z_+^2-z_-^2)}, \tag{A·22}$$

$$\frac{\partial z_\pm^2}{\partial \sigma_2} = \pm\frac{1}{z_+^2 - z_-^2}. \tag{A·23}$$

Derivatives of the elliptic integrals are given by

$$\frac{\partial {\rm F}(\varphi,k)}{\partial k} = \frac{1}{k}\left[\Pi(\varphi,k^2,k) - {\rm F}(\varphi,k)\right], \tag{A·24}$$

$$\frac{\partial \Pi(\varphi,n,k)}{\partial \varphi} = \frac{1}{(1-n\sin^2\varphi)\Delta_\varphi}\,, \tag{A·25}$$

$$\frac{\partial \Pi(\varphi,n,k)}{\partial n} = \frac{1}{n}\left[\Pi_{21}(\varphi,n,k) - \Pi(\varphi,n,k)\right], \tag{A·26}$$

$$\frac{\partial \Pi(\varphi,n,k)}{\partial k} = \frac{1}{k}\left[\Pi_{13}(\varphi,n,k) - \Pi(\varphi,n,k)\right], \tag{A·27}$$

with

$$\Pi_{ij}(\varphi,n,k) = \int_0^\varphi \frac{dx}{(1-n\sin^2 x)^i(1-k^2\sin^2 x)^{j/2}}\,. \tag{A·28}$$

A.2. *Meridian-plane orbits*

For the meridian-plane orbits for which $I_\varphi = 0$ ($\sigma_2 = 0$), the actions I_u and I_v defined by Eq. (2·3) can be simplified. In the dimensionless form (A·2) we obtain for the elliptic orbits,

$$\tilde{I}_u = 2\sqrt{\sigma}\ \mathrm{E}\left(\frac{1}{\sqrt{\sigma}}\right), \tag{A·29a}$$

$$\tilde{I}_v = \sqrt{\sigma}\left[\mathrm{E}\left(\theta_e,\frac{1}{\sqrt{\sigma}}\right) - \mathrm{E}\left(\frac{1}{\sqrt{\sigma}}\right)\right] + \frac{\sqrt{\eta^2-\sigma(\eta^2-1)}}{\eta\sqrt{\eta^2-1}}\,. \tag{A·29b}$$

Here we have used the identity[47)]

$$\Pi(\varphi,k^2,k) = \left[\mathrm{E}(\varphi,k) - k^2\sin\varphi\cos\varphi/\sqrt{1-k^2\sin^2\varphi}\right]/(1-k^2)\,. \tag{A·30}$$

In this subsection, we omit the suffix "1" on the variable σ_1 for brevity. For the hyperbolic orbits, we have

$$\tilde{I}_u = 2\left[\mathrm{E}(\sqrt{\sigma}) - (1-\sigma)\ \mathrm{F}(\sqrt{\sigma})\right], \tag{A·31a}$$

$$\tilde{I}_v = (1-\sigma)\left[\mathrm{F}(\sqrt{\sigma}) - \mathrm{F}(\theta_h,\sqrt{\sigma})\right] + \mathrm{E}(\theta_h,\sqrt{\sigma}) - \mathrm{E}(\sqrt{\sigma}) + \frac{\sqrt{\eta^2-\sigma(\eta^2-1)}}{\eta\sqrt{\eta^2-1}}. \tag{A·31b}$$

Equations (A·29) and (A·31) can be regarded as parametric equations in terms of the parameter σ for the energy surface of the meridian-plane orbits, $\varepsilon(\tilde{I}_u,\tilde{I}_v,\tilde{I}_\varphi=0)$, for its elliptic and hyperbolic parts, respectively.

The curvature K_{11} of the energy curve for the meridian-plane orbits can be obtained by differentiating Eqs. (A·29) and (A·31) implicitly through the parameter σ. In this way we obtain Eq. (3·13) with the dimensionless derivatives for the elliptic orbits

$$\frac{\partial \tilde{I}_u}{\partial \sigma} = \frac{1}{\sqrt{\sigma}}\ \mathrm{F}\left(\frac{1}{\sqrt{\sigma}}\right), \tag{A·32a}$$

$$\frac{\partial \tilde{I}_v}{\partial \sigma} = -\frac{1}{2\sqrt{\sigma}}\ \left[\mathrm{F}\left(\frac{1}{\sqrt{\sigma}}\right) - \mathrm{F}\left(\theta_e,\frac{1}{\sqrt{\sigma}}\right)\right], \tag{A·32b}$$

$$\frac{\partial^2 \tilde{I}_u}{\partial \sigma^2} = -\frac{1}{2\sqrt{\sigma^3}}\,\Pi\left(\frac{1}{\sigma}, \frac{1}{\sqrt{\sigma}}\right), \tag{A·32c}$$

$$\frac{\partial^2 \tilde{I}_v}{\partial \sigma^2} = \frac{1}{4\sqrt{\sigma^3}}\left[\Pi\left(\frac{1}{\sigma}, \frac{1}{\sqrt{\sigma}}\right) - \Pi\left(\theta_e, \frac{1}{\sigma}, \frac{1}{\sqrt{\sigma}}\right) + \frac{\eta\sqrt{\eta^2-1}}{\sqrt{1-(1-\sigma^{-1})\eta^2}}\right]. \tag{A·32d}$$

For the hyperbolic orbits, we have

$$\frac{\partial \tilde{I}_u}{\partial \sigma} = \mathrm{F}(\sqrt{\sigma}), \tag{A·33a}$$

$$\frac{\partial \tilde{I}_v}{\partial \sigma} = \frac{1}{2}\left[\mathrm{F}(\theta_h, \sqrt{\sigma}) - \mathrm{F}(\sqrt{\sigma})\right], \tag{A·33b}$$

$$\frac{\partial^2 \tilde{I}_u}{\partial \sigma^2} = \frac{1}{2\sigma}\left[\Pi(\sigma, \sqrt{\sigma}) - \mathrm{F}(\sqrt{\sigma})\right], \tag{A·33c}$$

$$\frac{\partial^2 \tilde{I}_v}{\partial \sigma^2} = \frac{1}{4\sigma}\left[\Pi(\theta_h, \sigma, \sqrt{\sigma}) - \Pi(\sigma, \sqrt{\sigma})z + \mathrm{F}(\sqrt{\sigma}) - \mathrm{F}(\theta_h, \sqrt{\sigma})\right]. \tag{A·33d}$$

Thus, for elliptic orbits, we obtain

$$\tilde{K}_{11} = \frac{1}{4\sqrt{\sigma^3}}\left[\frac{\mathrm{F}(\theta_e, \kappa)}{\mathrm{F}(\kappa)}\Pi(\kappa^2, \kappa) - \Pi(\theta_e, \kappa^2, \kappa) + \frac{\sqrt{\eta^2 - \sigma(\eta^2-1)}}{\eta\sqrt{\eta^2-1}}\right], \tag{A·34}$$

and for hyperbolic orbits,

$$\tilde{K}_{11} = -\frac{1}{4\sigma}\left[\frac{\mathrm{F}(\theta_h, \kappa)}{\mathrm{F}(\kappa)}\Pi(\kappa^2, \kappa) - \Pi(\theta_h, \kappa^2, \kappa)\right]. \tag{A·35}$$

A.3. *Equatorial-plane orbits*

For the equatorial limit $\sigma_2 = \sigma_1 \equiv \sigma$ we have, from (A·4),

$$z_-^2 = 0, \qquad z_+^2 = \sigma + 1\,. \tag{A·36}$$

We thus obtain in this limit ($k \to 0$)

$$\frac{\partial \tilde{I}_u}{\partial \sigma_1} = \frac{\pi}{2\sqrt{\sigma+1}}, \quad \frac{\partial \tilde{I}_v}{\partial \sigma_1} = -\frac{\varphi_{\mathrm{EQ}}}{2\sqrt{\sigma+1}}, \quad \frac{\partial z_\pm^2}{\partial \sigma_1} = \left\{\begin{matrix}\sigma/(\sigma+1)\\ 1/(\sigma+1)\end{matrix}\right\} \tag{A·37}$$

and

$$\frac{\partial^2 \tilde{I}_u}{\partial \sigma_1^2} = \frac{\pi(1-2\sigma)}{8(\sigma+1)^{5/2}},$$

$$\frac{\partial^2 \tilde{I}_v}{\partial \sigma_1^2} = \frac{1}{8(\sigma+1)^{5/2}}\left\{(2\sigma-1)\varphi_{\mathrm{EQ}} + \frac{1}{2}\sin(2\varphi_{\mathrm{EQ}}) - \frac{2\sqrt{\sigma+1}\left[z_b^2(1-\sigma) - (\sigma+1)\right]}{z_b^2\sqrt{z_b^2 - (\sigma+1)}}\right\},$$

$$\varphi_{\mathrm{EQ}} = \arcsin\frac{\sqrt{z_b^2 - (\sigma+1)}}{z_b}. \tag{A·38}$$

Substituting (A·37) and (A·38) into (A·9), we finally obtain the equatorial limit,

$$\tilde{K}_{11}^{\mathrm{EQ}} = \frac{z_b^2(2\sigma-1)+(\sigma+1)}{8z_b^2(\sigma+1)^2\sqrt{z_b^2-(\sigma+1)}}. \tag{A·39a}$$

In the same way, we obtain

$$\tilde{K}_{22}^{\mathrm{EQ}} = \frac{z_b^2(2-\sigma)+\sigma(\sigma+1)}{8z_b^2\sigma(\sigma+1)^2\sqrt{z_b^2-(\sigma+1)}}, \tag{A·39b}$$

$$\tilde{K}_{12}^{\mathrm{EQ}} = \frac{3z_b^2-(\sigma+1)}{8z_b^2(\sigma+1)^2\sqrt{z_b^2-(\sigma+1)}}. \tag{A·39c}$$

The determinant of the curvature matrix for EQPO becomes

$$\det \tilde{K}^{\mathrm{EQ}} = -\frac{1}{32z_b^2\sigma(\sigma+1)^2}, \tag{A·40}$$

which is negative for any orbit and for any deformation $\eta > 1$. This shows that bifurcations of EQPO occur only through the zeros of the stability factor F_z^{EQ}.

Appendix B

Derivation of the Trace Formula for the Equatorial-Plane Orbits

We start with the phase-space trace formula[9),28),31),40)]

$$\delta g_{\mathrm{scl}}(\varepsilon) = \mathrm{Re}\sum_{\alpha}\int \frac{d\boldsymbol{q}''d\boldsymbol{p}'}{(2\pi\hbar)^3}\,\delta\left(\varepsilon - H\left(\boldsymbol{q}',\boldsymbol{p}'\right)\right)\left|\mathcal{J}\left(\boldsymbol{p}_\perp'',\boldsymbol{p}_\perp'\right)\right|^{1/2} \times \exp\left\{\frac{i}{\hbar}\left[S_\alpha\left(\boldsymbol{p}',\boldsymbol{p}'',t_\alpha\right)+\left(\boldsymbol{p}''-\boldsymbol{p}'\right)\cdot\boldsymbol{q}''\right]-i\frac{\pi}{2}\nu_\alpha\right\}, \tag{B·1}$$

where the sum runs over all trajectories α, $\boldsymbol{q} = \boldsymbol{q}_\alpha(t,\boldsymbol{q}'',\boldsymbol{p}')$ determined by the fixed initial momentum $\boldsymbol{p}'$ and the final coordinate $\boldsymbol{q}''$, $H(\boldsymbol{q},\boldsymbol{p})$ is the classical Hamiltonian, and ν_α is the phase related to the Maslov index, number of caustics and turning points.[39),41)–43)] The function $S_\alpha(\boldsymbol{p}',\boldsymbol{p}'',t_\alpha)$ is the action in the mixed phase-space representation,

$$S_\alpha\left(\boldsymbol{p}',\boldsymbol{p}'',t_\alpha\right) = -\int_{\boldsymbol{p}'}^{\boldsymbol{p}''} d\boldsymbol{p}\cdot\boldsymbol{q}\left(\boldsymbol{p}\right), \tag{B·2}$$

related to the standard definition of the action $S_\alpha(\boldsymbol{q}',\boldsymbol{q}'',\varepsilon)$,

$$S_\alpha\left(\boldsymbol{q}',\boldsymbol{q}'',\varepsilon\right) = \int_{\boldsymbol{q}'}^{\boldsymbol{q}''} d\boldsymbol{q}\cdot\boldsymbol{p}\left(\boldsymbol{q}\right), \tag{B·3}$$

by the Legendre transformations (integration by parts),

$$S_\alpha\left(\boldsymbol{p}',\boldsymbol{p}'',t_\alpha\right) = S_\alpha\left(\boldsymbol{q}',\boldsymbol{q}'',\varepsilon\right)+\left(\boldsymbol{p}'-\boldsymbol{p}''\right)\boldsymbol{q}'', \tag{B·4}$$

t_α being the time for a particle to revolve the trajectory α. The quantity $\mathcal{J}\left(\boldsymbol{p}''_\perp, \boldsymbol{p}'_\perp\right)$ in Eq. (B·1) is the Jacobian for the transformation from $\boldsymbol{p}''_\perp$ to $\boldsymbol{p}'_\perp$. Here, we have introduced the local system of the phase-space coordinates $\boldsymbol{q} = \left\{q_\parallel, \boldsymbol{q}_\perp\right\}$ and $\boldsymbol{p} = \left\{p_\parallel, \boldsymbol{p}_\perp\right\}$, splitting the vectors into the parallel and perpendicular components with respect to the trajectory α.

For the equatorial-plane periodic orbits (EQPO), one of the components in $\boldsymbol{q}_\perp$ and $\boldsymbol{p}_\perp$ can be taken along the symmetry axis, say z and p_z, keeping for other perpendicular components the same suffix, $q_\perp$ and $p_\perp$. After the transformation to this local phase-space coordinate system and integration over the "parallel" momentum $p_\parallel = p = \sqrt{2m\varepsilon}$ by using the δ-function in Eq. (B·1), we obtain, for the contribution from the EQPO ($\mathcal{K} = 1$),

$$\delta g^{(1)}_{\rm EQ}(\varepsilon) = \frac{1}{(2\pi\hbar)^3}\,{\rm Re}\sum_\alpha \int \frac{dq''_\parallel}{|\dot q''_\parallel|}\int dq''_\perp dp'_\perp \int dz'' dp'_z \left|\mathcal{J}\left(\boldsymbol{p}'', \boldsymbol{p}'\right)\right|^{1/2} \times \exp\left\{\frac{i}{\hbar}\left[S_\alpha\left(\boldsymbol{p}', \boldsymbol{p}'', t_\alpha\right) + \left(\boldsymbol{p}'' - \boldsymbol{p}'\right)\cdot\boldsymbol{q}''\right] - i\frac{\pi}{2}\nu_\alpha\right\}, \tag{B·5}$$

where $\dot q_\parallel = \partial H/\partial p_\parallel = p/m$ is the velocity. In spheroidal action-angle variables, $q_\parallel = \Theta_v$, $p_\parallel = I_v$, $\dot q_\parallel = \omega_v$, $q_\perp = \Theta_\varphi = \varphi$, $p_\perp = I_\varphi$, $z = \Theta_u$, $p_z = I_u$, and we have

$$\delta g^{(1)}_{\rm EQ}(\varepsilon) = \frac{1}{(2\pi\hbar)^3}\,{\rm Re}\sum_\alpha \int \frac{d\Theta''_v}{|\omega_v|}\int d\Theta''_\varphi\, dI'_\varphi \int d\Theta''_u\, dI'_u \left|\mathcal{J}\left(I''_\varphi I''_u, I'_\varphi I'_u\right)\right|^{1/2} \times \exp\left\{\frac{i}{\hbar}\left[S_\alpha\left(\boldsymbol{I}', \boldsymbol{I}'', t_\alpha\right) + \left(\boldsymbol{I}'' - \boldsymbol{I}'\right)\cdot\boldsymbol{\Theta}''\right] - i\frac{\pi}{2}\nu_\alpha\right\}. \tag{B·6}$$

We now perform the integrations using the expansion of the action S_α about the stationary points:

$$S_\alpha\left(\boldsymbol{I}', \boldsymbol{I}'', t_\alpha\right) + \left(\boldsymbol{I}'' - \boldsymbol{I}'\right)\cdot\boldsymbol{\Theta}'' = S_\beta(\varepsilon) + \frac{1}{2}\sum_{ij} J_{ij}(\sigma_i - \sigma_i^*)(\sigma_j - \sigma_j^*) + \frac{1}{2}J_\perp\left(z - z^*\right)^2 + \cdots. \tag{B·7}$$

Here, we omit the corrections associated with mixed derivatives of type $\partial^2 S/\partial\Theta\partial I$ for simplicity. $J_\perp$ is the Jacobian corresponding to the second variation of the action S_α with respect to the angle variable Θ_u:

$$J^{\rm EQ}_\perp = \left(\frac{\partial^2 S_\alpha}{\partial {\Theta'_u}^2} + 2\frac{\partial^2 S_\alpha}{\partial\Theta'_u\partial\Theta''_u} + \frac{\partial^2 S_\alpha}{\partial {\Theta'_u}^2}\right)_{\rm EQ} = \left(-\frac{\partial I'_u}{\partial\Theta'_u} - 2\frac{\partial I'_u}{\partial\Theta''_u} + \frac{\partial I''_u}{\partial\Theta''_u}\right)_{\rm EQ}. \tag{B·8}$$

This quantity can be expressed in terms of the curvatures $K^{\rm EQ}$ and the Gutzwiller stability factor $F_z^{\rm EQ}$,

$$F_z^{\rm EQ} = -\left[\left(-\frac{\partial I'_u}{\partial\Theta'_u} - 2\frac{\partial I'_u}{\partial\Theta''_u} + \frac{\partial I''_u}{\partial\Theta''_u}\right)\Big/\frac{\partial I'_u}{\partial\Theta''_u}\right]_{\rm EQ} = 4\sin^2\left[\frac{1}{2}Mn_v\arccos\left(1 - 2\eta^{-2}\sin^2\phi\right)\right], \tag{B·9}$$

as

$$J_{\perp}^{\mathrm{EQ}} = -\frac{F_z^{\mathrm{EQ}}}{(J_u - J_{u\varphi}^2/J_\varphi)^{\mathrm{EQ}}} = -\frac{F_z^{\mathrm{EQ}}}{2\pi M n_v (K_u - K_{u\varphi}^2/K_\varphi)^{\mathrm{EQ}}}\,. \tag{B·10}$$

In these equations we have used the simple identical Jacobian transformations

$$\left(\frac{\partial I'_u}{\partial \Theta''_u}\right)^{-1}_{I'_\varphi} = \frac{\partial(\Theta''_u, I'_\varphi)}{\partial(I'_u, I'_\varphi)} = \frac{\partial \Theta''_u}{\partial I'_u} - \frac{\partial \Theta''_u}{\partial I'_\varphi}\frac{\partial I'_\varphi}{\partial I'_u} = J_u - J_{u\varphi}\frac{J_{u\varphi}}{J_\varphi}\,.$$

The curvature K_u^{EQ} is the quantity K_u defined in (B·13), evaluated at the stationary point $\sigma_1 = \sigma_2 = \sigma^*$ given by Eq. (3·27), and so on.

The integrand of (B·6) does not depend on the angles $(\Theta_v,\ \Theta_\varphi)$, and we obtain simply $(2\pi)^2$ for the integration over these angle variables. We transform the integration variables (I_u, I_φ) into (σ_1, σ_2) to obtain simple integration limits, and integrate over (σ_1, σ_2) using the ISPM. In this way we obtain

$$\begin{aligned}\delta g_{\mathrm{EQ}}^{(1)}(\varepsilon) = \sqrt{\frac{\pi}{2\hbar^3}}\,\mathrm{Re}\sum_\beta e^{i(kL_\beta - \pi\nu_\beta/2)}\frac{1}{\omega_v}\left|\frac{\partial(I_u, I_\varphi)}{\partial(\sigma_1,\sigma_2)}\right|\sqrt{\frac{1}{J_\perp|\det J^{\mathrm{EQ}}|}} \\ \times \mathrm{erf}(\mathcal{Z}_\perp^-, \mathcal{Z}_\perp^+; \mathcal{Z}_1^-, \mathcal{Z}_1^+; \mathcal{Z}_2^-, \mathcal{Z}_2^+),\end{aligned} \tag{B·11}$$

where

$$\mathrm{erf}\left(x^-, x^+; y^-, y^+; z^-, z^+\right) = \left(\frac{2}{\sqrt{\pi}}\right)^3 \int_{x^-}^{x^+} dx \int_{y^-}^{y^+} dy \int_{z^-}^{z^+} dz\, e^{-x^2-y^2-z^2}. \tag{B·12}$$

Note that the integration limits for the internal integrals over y and z in $\mathrm{erf}\,(x^-, x^+; y^-, y^+; z^-, z^+)$ in general depend on the variable of the next integrations, $y^\pm = y^\pm(x)$ and $z^\pm = z^\pm(x, y)$. Here we define curvatures in the variables (I_u, I_φ) as

$$\begin{aligned}J_u = \frac{\partial^2 S_\alpha}{\partial I_u^2} = 2\pi M n_v K_u, \quad J_\varphi = \frac{\partial^2 S_\alpha}{\partial I_\varphi^2} = 2\pi M n_v K_\varphi, \\ J_{u\varphi} = \frac{\partial^2 S_\alpha}{\partial I_u \partial I_\varphi} = 2\pi M n_v K_{u\varphi}.\end{aligned} \tag{B·13}$$

Using (B·10) and the relations

$$\det J \equiv J_{11}J_{22} - {J_{12}}^2 = \left|\frac{\partial(I_u, I_\varphi)}{\partial(\sigma_1,\sigma_2)}\right|^2 (J_u J_\varphi - {J_{u\varphi}}^2), \tag{B·14}$$

$$K_\varphi = \frac{1}{\pi p a \sin\phi}, \qquad \omega_v = \frac{\pi p}{m a \sin\phi}, \tag{B·15}$$

we finally obtain

$$\delta g_{\mathrm{EQ}}^{(1)}(\varepsilon) = \frac{1}{\varepsilon_0}\,\mathrm{Re}\sum_{\mathrm{EQ}} A_{\mathrm{EQ}} \exp\left(ikL_{\mathrm{EQ}} - i\frac{\pi}{2}\nu_{\mathrm{EQ}}\right), \tag{B·16}$$

$$A_{\rm EQ}=\frac{1}{2}\sqrt{\frac{\sin^3\phi}{\pi M n_v k R\eta F_z}}\,{\rm erf}\left(\mathcal{Z}_\perp^-,\mathcal{Z}_\perp^+;\mathcal{Z}_1^-,\mathcal{Z}_1^+;\mathcal{Z}_2^-,\mathcal{Z}_2^+\right), \tag{B·17}$$

where $L_{\rm EQ}$ represents the length of the EQPO. The "triple" error function in Eq. (B·17) can be separated into the product of three standard error functions as

$${\rm erf}\left(\mathcal{Z}_\perp^-,\mathcal{Z}_\perp^+;\mathcal{Z}_1^-,\mathcal{Z}_1^+;\mathcal{Z}_2^-,\mathcal{Z}_2^+\right)\approx{\rm erf}\left(\mathcal{Z}_\perp^-,\mathcal{Z}_\perp^+\right){\rm erf}\left(\mathcal{Z}_1^-,\mathcal{Z}_1^+\right){\rm erf}\left(\mathcal{Z}_2^-,\mathcal{Z}_2^+\right) \tag{B·18}$$

by taking the limits at the stationary points for all deformations, except in a small region near the spherical shape. In this way, we obtain the simple results (3·30). The arguments of the error functions are given by (3·19) or (3·20) for $\mathcal{Z}_i^\pm$ $(i=1,2)$ and

$$\mathcal{Z}_\perp^\pm=\pm\frac{\pi}{2}\sqrt{-\frac{iJ_\perp^{\rm EQ}}{2\hbar}}=\pm\frac{\hbar(k\zeta)^2}{16}\sqrt{\frac{iF_z^{\rm EQ}}{Mn_v ka\sin\phi\,\sigma^*(\sigma^*+1)\det K^{\rm EQ}}}. \tag{B·19}$$

The spherical limit is easily obtained by using the spherical action-angle variables $\{\Theta_\theta,\Theta_r,\Theta_\varphi;I_\theta,I_r,I_\varphi\}$. In these variables,

$$A_{\rm EQ}=\frac{1}{2}\sqrt{\frac{\sin^3\phi}{\pi M n_r k R\eta F_z}}\,{\rm erf}\left(\mathcal{Z}_\perp^-,\mathcal{Z}_\perp^+;\mathcal{Z}_\theta^-,\mathcal{Z}_\theta^+;\mathcal{Z}_\varphi^-,\mathcal{Z}_\varphi^+\right), \tag{B·20}$$

where $n_r\equiv n_v$ for the equatorial-plane orbits with (n_v,n_φ), and the invariant stability factor $F_\theta\equiv F_z^{\rm EQ}$ is given by (B·9):

$$\mathcal{Z}_\perp^\pm=\sqrt{\frac{-i\pi F_\theta^{\rm EQ}}{16Mn_r\hbar K_\theta^{\rm EQ}}}(z^\pm-z^*),\quad \mathcal{Z}_{\{\theta\atop\varphi\}}^\pm=\sqrt{-i\pi Mn_r K_{\{\theta\atop\varphi\}}^{\rm EQ}/\hbar}\left(I_{\{\theta\atop\varphi\}}^\pm-I_{\{\theta\atop\varphi\}}^*\right). \tag{B·21}$$

The quantities $K_\theta^{\rm EQ}$ and $K_\varphi^{\rm EQ}$, given by

$$K_{\{\theta\atop\varphi\}}^{\rm EQ}=\left(\frac{\partial^2 I_r}{\partial I_{\{\theta\atop\varphi\}}^2}\right)_{\rm EQ}, \tag{B·22}$$

are the curvatures of the energy surface $\varepsilon=H(I_\theta,I_r,I_\varphi)$ in the spherical coordinate system. In that system, the maximum value of I_φ is equal to the absolute value of the classical angular momentum I_θ, $I_\varphi^\pm=\pm I_\theta$, I_θ^+ being the maximum value of $|I_\theta|$, and $I_\theta^-=0$. We note that for the diametric orbits, the stationary points I_θ^* and I_φ^* are exactly zero and there are also specific integration limits in Eq. (B·20). In this case, the internal integral over I_φ within a small region can be evaluated approximately as $2I_\theta$, and we obtain for the "triple" error function,

$${\rm erf}\left(\mathcal{Z}_\perp^-,\mathcal{Z}_\perp^+;\mathcal{Z}_\theta^-,\mathcal{Z}_\theta^+;\mathcal{Z}_\varphi^-,\mathcal{Z}_\varphi^+\right)\to\sqrt{\frac{-4iF_z}{M\pi^2 n_r\hbar K_\theta^{\rm EQ}}}=\sqrt{\frac{-4iF_z kR}{2\pi M}}. \tag{B·23}$$

Here, we have used the fact that in the spherical limit, $F_z \to 0$, the integral over $\mathcal{Z}_\theta$ can be approximated by the upper limit $\mathcal{Z}_\theta^+$ given by Eq. (B·21). We also omitted the strong oscillating value of $\int dz^2 e^{-z^2}$ at the upper limit, because it vanishes after any small averaging over kR and equals 1 in this approximation. We also accounted for the fact that $K_\theta^{\rm EQ} \to 1/(\pi pR)$ for the diameters (see Eq. (B·22) and note that $\phi = \pi/2$ for the diameters). Finally, the stability factor F_z is canceled, and we obtain the Balian-Bloch result (3·33) for the contribution of the diametric orbits in the spherical cavity.[3)]

For all other EQPO there are the stationary points $I_\varphi^* = I_\theta^* \neq 0$, and I_φ is identical to its maximum value I_θ in the spherical limit. This is the reason that there is no next order $(1/\sqrt{kR})$ corrections to the Balian-Bloch trace formula for the contribution of the planar orbits with $n_r \geq 3$. The latter comes from the spherical limit of the elliptic orbits in the meridian plane (3·16) (see Ref. 9)).

Appendix C
Separatrix

As in the case of the turning points,[39),41)–43)] we first expand the exponent phase in Eq. (3·6) with respect to I'_u:

$$S_\alpha\left(\boldsymbol{I}', \boldsymbol{I}'', t_\alpha\right) - \left(\boldsymbol{I}'' - \boldsymbol{I}'\right) \cdot \boldsymbol{\Theta}'' = c_0^{\parallel} + c_1^{\parallel} x + c_2^{\parallel} x^2 + c_3^{\parallel} x^3 + \cdots \equiv \tau_0^{\parallel} + \tau_1^{\parallel} z + \frac{1}{3} z^3. \tag{C·1}$$

Here,

$$x = \frac{1}{\hbar}\left(I'_u - I'^{\,*}_u\right), \tag{C·2}$$

$$c_0^{\parallel} = \frac{1}{\hbar}\left[S_\alpha^*\left(\boldsymbol{I}', \boldsymbol{I}'', \varepsilon\right) - \left(\boldsymbol{I}' - \boldsymbol{I}''\right)^* \cdot \boldsymbol{\Theta}''^*\right] = \frac{1}{\hbar} S_\alpha^*\left(\boldsymbol{\Theta}', \boldsymbol{\Theta}'', \varepsilon\right), \tag{C·3}$$

$$c_1^{\parallel} = \left(\frac{\partial S_\alpha}{\partial I'_u} - \Theta''_u\right)^* = \Theta'_u - \Theta''_u \to 0, \qquad \sigma_1 \to 1, \tag{C·4}$$

$$c_2^{\parallel} = \frac{\hbar}{2}\left(\frac{\partial^2 S_\alpha}{\partial I'^{\,2}_u}\right)^* = 2p\zeta M \hbar \tilde{K}_u^\alpha \to \infty, \qquad \sigma_1 \to 1, \tag{C·5}$$

$$c_3^{\parallel} = \frac{\hbar^3}{6}\left(\frac{\partial^3 S_\alpha}{\partial I'^{\,3}_u}\right)^* = \frac{2\pi^3 \hbar^2 M}{3(p\zeta^2)^2}\left(\frac{\partial \tilde{K}_u^\alpha}{\partial \tilde{I}_u}\right) < 0, \quad \sigma_\parallel \to 1, \tag{C·6}$$

where the superscript asterisk indicates the value at $I'_u = I''_u = I^*_u$. The asymptotic behavior of the constants $c_i^{\parallel}$ near the separatrix $\sigma_1 \approx 1$ is found from

$$\tilde{K}_u^\alpha \to \frac{\log\left[(1+\sin\theta)/(1-\sin\theta)\right]}{(\sigma_1 - 1)\log^3(\sigma_1 - 1)}, \qquad \sigma_1 \to 1, \tag{C·7}$$

and with $\theta \to \theta_h(\eta)$ [see Eq. (2·6)],

$$\frac{\partial \tilde{K}_u^\alpha}{\partial \tilde{I}_u} \to -\frac{2\log\left[(1+\sin\theta)/(1-\sin\theta)\right]}{\left((\sigma_1 - 1)\log^2(\sigma_1 - 1)\right)^2}, \qquad \sigma_1 \to 1. \tag{C·8}$$

The rightmost part of Eq. (C·1) is obtained using a linear transformation with some constants α and β:

$$x = \alpha z + \beta, \qquad \alpha = \left(3c_3^{\|}\right)^{-1/3}, \qquad \beta = -c_2^{\|}/(3c_3^{\|}), \tag{C·9}$$

$$\tau_0^{\|} = \left(c_0 - c_1c_2/(3c_3) + 2c_2^3/(27c_3^2)\right)^{\|}, \qquad \tau_1^{\|} = \alpha\left[c_1 - c_2^2/(3c_3)\right]^{\|}. \tag{C·10}$$

Near the stationary point for $\sigma_1 \to 1$, we obtain $c_1^{\|} \to 0$ and $\tau_1^{\|} \to -w^{\|}$, with the positive quantity

$$w^{\|} = \left(\frac{c_2^2}{(3c_3)^{4/3}}\right)^{\|} \to \left|\frac{M\log\left[(1+\sin\theta)/(1-\sin\theta)\right](\sigma_1-1)}{\hbar\log(\sigma_1-1)}\right|^{2/3}. \tag{C·11}$$

Using expansion (C·1) in Eq. (3·6) and evaluating the integral over Θ_v'' exactly (i.e., obtaining a factor of 2π for this integral), we obtain

$$\begin{aligned}\delta g_{\rm LD}^{(0)} &= -\frac{2}{2\pi\hbar^2}\,{\rm Re}\sum_\alpha\int d\Theta_\varphi''\int dI_\varphi'\int d\Theta_u''\frac{1}{|\omega_v^*|}e^{i\left(\tau_0^{\|}-\frac{\pi}{2}\nu_\alpha\right)}\\ &\quad\times\sqrt{\frac{\sqrt{w^{\|}}}{c_2^{\|}}}\left[{\rm Ai}\left(-w^{\|},\mathcal{Z}_{\|}^-,\mathcal{Z}_{\|}^+\right)+i\,{\rm Gi}\left(-w^{\|},\mathcal{Z}_{\|}^-,\mathcal{Z}_{\|}^+\right)\right]\\ &\approx -\frac{2}{\hbar}\,{\rm Re}\sum_\alpha\int d\Theta_u''\frac{1}{|\omega_v^*|}\sqrt{\frac{\sqrt{w^{\|}}}{c_2^{\|}}}\left[{\rm Ai}\left(-w^{\|}\right)+i\,{\rm Gi}\left(-w^{\|}\right)\right]e^{i\left(\tau_0^{\|}-\frac{\pi}{2}\nu_\alpha\right)},\end{aligned} \tag{C·12}$$

where

$$\mathcal{Z}_{\|}^- = \sqrt{w^{\|}}, \qquad \mathcal{Z}_{\|}^+ = \sqrt{\frac{c_2^{\|}}{\sqrt{w^{\|}}}\frac{I_u^{\rm (cr)}}{\hbar}} + \sqrt{w^{\|}}. \tag{C·13}$$

Here, ${\rm Ai}(-w,z_1,z_2)$ and ${\rm Gi}(-w,z_1,z_2)$ are the incomplete Airy and Gairy functions defined by

$$\left\{\begin{matrix}{\rm Ai}\\ {\rm Gi}\end{matrix}\right\}(-w,z_1,z_2) = \frac{1}{\pi}\int_{z_1}^{z_2}dz\,\left\{\begin{matrix}\cos\\ \sin\end{matrix}\right\}\left(-wz+\frac{z^3}{3}\right), \tag{C·14}$$

${\rm Ai}(-w)$ and ${\rm Gi}(-w)$ are the corresponding standard complete functions, and $I_u^{\rm (cr)} = I_u(\sigma_1^{\rm (cr)},\sigma_1^{\rm (cr)})$ is the "creeping" elliptic 2DPO value defined in §2. In the second equality of (C·12), we have used

$$\begin{aligned}&\mathcal{Z}_{\|}^- \to 0,\\ &\mathcal{Z}_{\|}^+ \to 4\left[\frac{M\log\left[(1+\sin\theta)/(1-\sin\theta)\right]p\zeta}{2(\sigma_1-1)^2\log^4(\sigma_1-1)}\right]^{1/3}\left[\frac{\eta}{\sqrt{\eta^2-1}}{\rm E}\left(\frac{\sqrt{\eta^2-1}}{\eta}\right)-1\right]\\ &\qquad\to\infty,\end{aligned} \tag{C·15}$$

for any finite deformation η and large kR near the separatrix ($\sigma_1 \to 1$). Using an analogous expansion of the action $\tau_0^{\parallel}$ in (C·12) with respect to the angle Θ_u'' to third order and a linear transformation like (C·9), we arrive at

$$\begin{aligned}\delta g_{\rm LD}^{(0)}(\varepsilon) = {} & \frac{b}{2\varepsilon_0 \pi^2 R\hbar}\,{\rm Re}\sum_\alpha \int d\Theta_\varphi'' \int dI_\varphi' \frac{1}{kR}\frac{\left(w^{\parallel}w^{\perp}\right)^{1/4}}{\sqrt{|c_2^{\parallel}c_2^{\perp}|}} \\ & \times \left[{\rm Ai}\left(-w^{\parallel}\right) + i\,{\rm Gi}\left(-w^{\parallel}\right)\right]\left[{\rm Ai}\left(-w^{\perp},\mathcal{Z}_{\perp}^{-},\mathcal{Z}_{\perp}^{+}\right) + i\,{\rm Gi}\left(-w^{\perp},\mathcal{Z}_{\perp}^{-},\mathcal{Z}_{\perp}^{+}\right)\right] \\ & \times \exp\left\{\frac{i}{\hbar}\left[S_\alpha^*\left(\boldsymbol{I}',\boldsymbol{I}'',\varepsilon\right) - \left(\boldsymbol{I}'-\boldsymbol{I}''\right)^*\cdot\boldsymbol{\Theta}''^*\right]\right. \\ & \left. + \frac{2i}{3}\left[(w^{\parallel})^{3/2} + (w^{\perp})^{3/2}\right] - i\frac{\pi}{2}\nu_\alpha\right\}, \end{aligned} \tag{C·16}$$

where

$$w^{\perp} = \left(\frac{c_2^2}{(3c_3)^{4/3}}\right)^{\perp} > 0, \tag{C·17}$$

$$\mathcal{Z}_{\perp}^{-} = \sqrt{w^{\perp}}, \qquad \mathcal{Z}_{\perp}^{+} = \frac{\pi}{2}\left|3c_3^{\perp}\right|^{1/3} + \sqrt{w^{\perp}}, \tag{C·18}$$

$$c_2^{\perp} = \frac{1}{2\hbar}\left(J_{u,\alpha}^{\perp}\right)^* = \left(\frac{\partial^2 S_\alpha}{\partial\Theta_u'^2} + 2\frac{\partial^2 S_\alpha}{\partial\Theta_u'\partial\Theta_u''} + \frac{\partial^2 S_\alpha}{\partial\Theta_u''^2}\right)_{\rm LD}^{*} = -\frac{F_{xy}^{\rm LD}}{2\pi M K_u^{\alpha}}. \tag{C·19}$$

Here, $F_{xy}^{\rm LD}$ is the stability factor for long diameters,

$$F_{xy}^{\rm LD} = -4\sinh^2\left[M\,{\rm arccosh}\left(2\eta^2-1\right)\right], \tag{C·20}$$

$$\begin{aligned} c_3^{\perp} &= \frac{1}{6\hbar}\left[\frac{\partial^3 S_\alpha}{\partial\Theta_u'^3} + 3\frac{\partial^3 S_\alpha}{\partial\Theta_u'^2\partial\Theta_u''} + 3\frac{\partial^3 S_\alpha}{\partial\Theta_u'\partial\Theta_u''^2} + \frac{\partial^3 S_\alpha}{\partial\Theta_u''^3}\right]^* \\ &= \frac{1}{6\hbar}\left[\frac{\partial J_{u,\alpha}^{\perp}}{\partial\Theta_u'} + \frac{\partial J_{u,\alpha}^{\perp}}{\partial\Theta_u''}\right]^* < 0\,. \end{aligned} \tag{C·21}$$

Note that according to (C·19), the quantity $c_2^{\perp}$ approaches zero near the separatrix ($\sigma_1 \to 1$) as in the caustic case. This is the reason that we apply the Maslov-Fedoryuk theory[39),41)–43)] for the transformation of the integral over the angle Θ_u'' from (C·12) to (C·16). The remaining two integrals over the azimuthal variables (I_φ' and Θ_φ'') can be calculated in a manner similar to that explained in the text.

The divergence of the curvature K_φ, Eq. (B·13), for the long diameters ($\sigma_1 \to 1$, $\sigma_2 \to 0$) can be easily seen from the following expression, valid for any polygon orbit with a vertex on the symmetry axis:

$$K_\varphi^{\beta} = \frac{L_0 c}{\rho_0^2 n_v M\hbar}\left[\frac{2\eta^2}{1+\eta^2\tan^2\psi} - 1\right]. \tag{C·22}$$

Here, L_0 denotes the length of the side having a vertex at the pole, ρ_0 the cylindrical coordinate of the other end of this side, and ψ the angle between this side and the symmetry axis. For the long diameters, $L_0 \to 2bM$, $\rho_0 \to 0$ and $\psi \to 0$, so that $K_\varphi^{\beta} \to \infty$.

Appendix D
Derivation of the Third-Order Term

D.1. *Third-order curvatures*

For the curvature $K_1^{(3)}$, which appears in the third-order terms in the expansion of the action $S/\hbar$ with respect to σ_1, we obtain

$$\tilde{K}_1^{(3)} = \frac{\pi}{p\zeta} K_1^{(3)} = \frac{\partial^3 \tilde{I}_v}{\partial \sigma_1^3} + \frac{n_u}{n_v} \frac{\partial^3 \tilde{I}_u}{\partial \sigma_1^3}, \tag{D·1}$$

where

$$\begin{aligned} \frac{\partial^3 \tilde{I}_v}{\partial \sigma_1^3} &= -\frac{1}{4z_+^3} \left[\frac{\partial B_v}{\partial \sigma_1} + 6z_+ \frac{\partial z_+^2}{\partial \sigma_1} \frac{\partial^2 \tilde{I}_v}{\partial \sigma_1^2} \right], \\ \frac{\partial^3 \tilde{I}_u}{\partial \sigma_1^3} &= \frac{1}{2z_+^3} \left[\frac{\partial B_u}{\partial \sigma_1} - 3z_+ \frac{\partial z_+^2}{\partial \sigma_1} \frac{\partial^2 \tilde{I}_u}{\partial \sigma_1^2} \right], \end{aligned} \tag{D·2}$$

$$B_v = \left[\Pi(\varphi, k^2, k) - \mathrm{F}(\varphi, k) \right] \tilde{\partial}_k - \frac{\partial z_+^2}{\partial \sigma_1} \mathrm{F}(\varphi, k) + \frac{2z_+^2}{\Delta_\varphi} \frac{\partial \varphi}{\partial \sigma_1}, \tag{D·3}$$

$$\begin{aligned} B_u &= \left[\Pi(k^2, k) - \mathrm{F}(k) \right] \tilde{\partial}_k - \frac{\partial z_+^2}{\partial \sigma_1} \mathrm{F}(k), \\ \tilde{\partial}_k &= \frac{z_+^2}{k^2} \frac{\partial k^2}{\partial \sigma_1} = \frac{1}{k^2} \frac{\partial z_-^2}{\partial \sigma_1} - \frac{\partial z_+^2}{\partial \sigma_1}, \end{aligned} \tag{D·4}$$

with the derivatives

$$\begin{aligned} \frac{\partial B_u}{\partial \sigma_1} &= k \left[\frac{\partial \Pi(k^2, k)}{\partial \partial k} - \frac{\partial \mathrm{F}(k)}{\partial k} \right] \frac{\tilde{\partial}_k^2}{2z_+^2} + \left[\Pi(k^2, k) - \mathrm{F}(k) \right] \left[-\frac{\tilde{\partial}_k}{z_-^2} \frac{\partial z_-^2}{\partial \sigma_1} \right. \\ &\quad \left. + \frac{1}{k^2} \frac{\partial^2 z_-^2}{\partial \sigma_1^2} - \frac{\partial^2 z_+^2}{\partial \sigma_1^2} \right] - k \frac{\partial \mathrm{F}(k)}{\partial k} \frac{\tilde{\partial}_k}{2z_+^2} \frac{\partial z_+^2}{\partial \sigma_1} - \frac{\partial^2 z_+^2}{\partial \sigma_1^2} \mathrm{F}(k), \\ \frac{\partial^2 z_\pm^2}{\partial \sigma_1^2} &= \pm \frac{2\sigma_2}{\left[(\sigma_1 - 1)^2 + 4\sigma_2 \right]^{3/2}}, \end{aligned} \tag{D·5}$$

$$\begin{aligned} \frac{\partial B_v}{\partial \sigma_1} &= \tilde{\partial}_k \left[\frac{\partial \Pi(\varphi, k^2, k)}{\partial \sigma_1} - \frac{\partial \mathrm{F}(\varphi, k)}{\partial \sigma_1} + \left(1 - \frac{1}{z_-^2} \frac{\partial z_-^2}{\partial \sigma_1} \right) \right] - \frac{\partial^2 z_+^2}{\partial \sigma_1^2} \mathrm{F}(\varphi, k) \\ &\quad - \frac{\partial z_-^2}{\partial \sigma_1} \frac{\partial \mathrm{F}(\varphi, k)}{\partial \sigma_1} + \frac{1}{\Delta_\varphi} \left[\left(2 \frac{\partial z_+^2}{\partial \sigma_1} - \frac{z_+^2}{\Delta_\varphi^2} \frac{\partial \Delta_\varphi^2}{\partial \sigma_1} \right) \frac{\partial \varphi}{\partial \sigma_1} + 2z_+^2 \frac{\partial^2 \varphi}{\partial \sigma_1^2} \right]. \end{aligned} \tag{D·6}$$

Here,

$$\frac{\partial \Pi(k^2, k)}{\partial k} = \frac{k^2 \tilde{\partial}_k}{k_1^2 z_+^2} \left[\Pi(k^2, k) + \frac{1}{2k^2} \left(\mathrm{E}(k) - \mathrm{F}(k) \right) \right], \tag{D·7}$$

$$\frac{\partial \mathrm{F}(k)}{\partial k} = \frac{1}{k}\left[\Pi(k^2,k) - \mathrm{F}(k)\right], \tag{D·8}$$

$$\frac{\partial \Pi(\varphi,k^2,k)}{\partial \sigma_1} = \frac{1}{k_1^2}\left[\frac{k^2\tilde{\partial}_k}{z_+^2}\left\{\Pi(\varphi,k^2,k) + \frac{1}{2k^2}\left(\mathrm{E}(\varphi,k) - \mathrm{F}(\varphi,k)\right)\right.\right.$$
$$\left.\left. - \frac{\sin(2\varphi)}{4\Delta_\varphi^3}\left(1+\Delta_\varphi^2\right)\right\} + \Delta_\varphi \frac{\partial \varphi}{\partial \sigma_1}\left\{1 - \frac{k^2}{4\Delta_\varphi^4}\left[4\Delta_\varphi^2\cos(2\varphi) + k^2\sin^2(2\varphi)\right]\right\}\right], \tag{D·9}$$

$$\frac{\partial \mathrm{F}(\varphi,k)}{\partial \sigma_1} = \frac{\tilde{\partial}_k}{2z_+^2}\left[\Pi(\varphi,k^2,k) - \mathrm{F}(\varphi,k)\right] + \frac{1}{\Delta_\varphi}\frac{\partial \varphi}{\partial \sigma_1}, \tag{D·10}$$

$$\frac{\partial^2 \varphi}{\partial \sigma_1^2} = \frac{1}{\sin(2\varphi)}\left\{\frac{1}{\left(z_b^2 - z_-^2\right)^3}\left[\left(\frac{\partial^2 z_-^2}{\partial \sigma_1^2}\left(z_b^2 - z_+^2\right) - \frac{\partial^2 z_+^2}{\partial \sigma_1^2}\left(z_b^2 - z_-^2\right)\right)\right.\right.$$
$$\left.\left. + 2\frac{\partial z_-^2}{\partial \sigma_1}\left(\frac{\partial z_-^2}{\partial \sigma_1}\left(z_b^2 - z_+^2\right) - \frac{\partial z_+^2}{\partial \sigma_1}\left(z_b^2 - z_-^2\right)\right)\right] - 2\cos(2\varphi)\left(\frac{\partial \varphi}{\partial \sigma_1}\right)^2\right\}, \tag{D·11}$$

$$\frac{\partial \Delta_\varphi^2}{\partial \sigma_1} = -k^2\left[\frac{\tilde{\partial}_k}{z_+^2}\sin^2\varphi + \sin(2\varphi)\frac{\partial \varphi}{\partial \sigma_1}\right]. \tag{D·12}$$

D.2. *Stationary phase method with third-order expansions*

After the expansion of the action in the Poisson-sum trace formula (3·10) up to second order with respect to σ_2 and up to third order with respect to σ_1, we obtain

$$\delta g^{(2)}(\varepsilon) = \frac{k\zeta^2}{4\pi^2 R\varepsilon_0}\,\mathrm{Re}\sum_\beta \frac{L_\beta}{M n_v R\sqrt{\sigma_2^*}}\left(\frac{\partial \tilde{I}_u}{\partial \sigma_1}\right)^* \exp\left(ikL_\beta - i\frac{\pi}{2}\nu_\beta\right)$$
$$\times \int_0^{\sigma_2^+} d\sigma_2 \int_{x^-}^{x^+} dx\, \exp\left[ik\zeta M n_v \tilde{K}_{22}\left(\sigma_2 - \sigma_2^* + \frac{K_{12}}{K_{22}}(\sigma_1 - \sigma_1^*)\right)^2\right.$$
$$\left. + i\left(c_1 x + c_2 x^2 + c_3 x^3\right)\right], \tag{D·13}$$

where

$$c_1 \to 0, \quad c_2 = k\zeta M n_v \frac{\det \tilde{K}}{\tilde{K}_{22}}, \quad c_3 = \frac{1}{3}k\zeta M n_v \tilde{K}_1^{(3)}, \tag{D·14}$$

$$x = \sigma_1 - \sigma_1^*, \quad x^\pm = \sigma_1^\pm - \sigma_1^*. \tag{D·15}$$

After transformation from σ_2 to the new variable $\mathcal{Z}_2$, defined by

$$\mathcal{Z}_2 = \sqrt{-ik\zeta M n_v \tilde{K}_{22}}\left(\sigma_2 - \sigma_2^* + \frac{K_{12}}{K_{22}}(\sigma_1 - \sigma_1^*)\right), \tag{D·16}$$

and a linear transformation from x to z through

$$x = q_1 z + q_2, \quad \text{with} \quad q_1 = (3c_3)^{-1/3}, \quad q_2 = -\frac{c_2}{3c_3}, \tag{D·17}$$

we obtain Eq. (3·15) with the ISPM3 amplitude

$$A_{3\mathrm{D}}^{(2)}(\varepsilon) = \frac{L_\beta}{8Mn_vR\left(k\zeta Mn_v\tilde{K}_1^{(3)}\right)^{1/3}}\sqrt{\frac{ik\zeta^3}{\pi Mn_vR^2\tilde{K}_{22}\sigma_2^*}}\left(\frac{\partial\tilde{I}_u}{\partial\sigma_1}\right)^*\exp\left(\frac{2}{3}i\tau^{3/2}\right)$$
$$\times\,\mathrm{erf}\left(\mathcal{Z}_2^-,\mathcal{Z}_2^+\right)\left[\mathrm{Ai}\left(-\tau,z_-,z_+\right)+i\,\mathrm{Gi}\left(-\tau,z_-,z_+\right)\right]. \tag{D·18}$$

Here, $\mathcal{Z}_2^\pm$ is defined by Eq. (3·20b), and

$$\tau=(3c_3)^{-1/3}\left(\frac{c_2^2}{3c_3}-c_1\right),\quad z_\pm=\frac{x^\pm-q_2}{q_1}. \tag{D·19}$$

In the limit $c_1\to 0$, we obtain

$$\tau=\frac{c_2^2}{(3c_3)^{4/3}}=\frac{(k\zeta Mn_v)^{2/3}(\det\tilde{K}/\tilde{K}_{22})^2}{\left(\tilde{K}_1^{(3)}\right)^{4/3}}. \tag{D·20}$$

For finite curvatures far from the bifurcations, the limits of the Airy and Gairy functions can be extended as $z_-\to 0$ and $z_+\to\infty$, yielding the complete Airy $\mathrm{Ai}(-\tau)$ and Gairy $\mathrm{Gi}(-\tau)$ functions. Then, using the asymptotic forms of these functions for large $\tau\propto(kR)^{2/3}$ (large kR),

$$\left\{\begin{matrix}\mathrm{Ai}\\ \mathrm{Gi}\end{matrix}\right\}(-\tau)\sim\frac{1}{\sqrt{\pi}\tau^{1/4}}\left\{\begin{matrix}\sin\\ \cos\end{matrix}\right\}\left(\frac{2}{3}\tau^{3/2}+\frac{\pi}{4}\right), \tag{D·21}$$

and that of the erf-function given in Eq. (D·18), we obtain the SSPM limit, (3·21).

References

1) M. C. Gutzwiller, J. Math. Phys. **12** (1971), 343; and earlier references quoted therein.
2) M. C. Gutzwiller, *Chaos in Classical and Quantum Mechanics* (Springer-Verlag, New York, 1990).
3) R. B. Balian and C. Bloch, Ann. of Phys. **69** (1972), 76.
4) V. M. Strutinsky, Nukleonika **20** (1975), 679.
   V. M. Strutinsky and A. G. Magner, Sov. Phys. Part. Nucl. **7** (1977), 138.
5) M. V. Berry and M. Tabor, Proc. Roy. Soc. London A **349** (1976), 101.
6) M. V. Berry and M. Tabor, J. of Phys. A **10** (1977), 371.
7) S. C. Creagh and R. G. Littlejohn, Phys. Rev. A **44** (1990), 836; J. of Phys. A **25** (1992), 1643.
8) V. M. Strutinsky, A. G. Magner, S. R. Ofengenden and T. Døssing, Z. Phys. A **283** (1977), 269.
9) A. G. Magner, S. N. Fedotkin, F. A. Ivanyuk, P. Meier, M. Brack, S. M. Reimann and H. Koizumi, Ann. of Phys. **6** (1997), 555.
   A. G. Magner, S. N. Fedotkin, F. A. Ivanyuk, P. Meier and M. Brack, Czech. J. of Phys. **48** (1998), 845.
10) M. Brack and R. K. Bhaduri, *Semiclassical Physics* (Addison-Wesley, 1997).
11) H. Frisk, Nucl. Phys. A **511** (1990), 309.
12) K. Arita and K. Matsuyanagi, Nucl. Phys. A **592** (1995), 9.
13) M. Brack, S. M. Reimann and M. Sieber, Phys. Rev. Lett. **79** (1997), 1817.
    M. Brack, P. Meier, S. M. Riemann and M. Sieber, in *Similarities and Differences between Atomic Nuclei and Clusters*, ed. Y. Abe et al. (AIP, New York, 1998), p. 17.
14) H. Nishioka, K. Hansen and B. R. Mottelson, Phys. Rev. B **42** (1990), 9377.

15) M. Brack, S. Creag, P. Meier, S. Reimann and M. Seidl, in *Large Cluster of Atoms and Molecules*, ed. T. P. Martin (Kluwer, Dordrecht, 1996), p. 1.
M. Brack, J. Blaschke, S. C. Creag, A. G. Magner, P. Meier and S. M. Reimann, Z. Phys. D **40** (1997), 276.
16) S. Frauendorf, V. M. Kolomietz, A. G. Magner and A. I. Sanzhur, Phys. Rev. B **58** (1998), 5622.
17) S. M. Reimann, M. Persson, P. E. Lindelof and M. Brack, Z. Phys. B **101** (1996), 377.
18) J. Ma and K. Nakamura, Phys. Rev. B **60** (1999), 10676; ibid. **60** (1999), 11611.
19) J. Blaschke and M. Brack, Europhys. Lett. **50** (2000), 294.
20) J. Ma and K. Nakamura, Phys. Rev. B **62** (2000), 13552.
21) J. Ma and K. Nakamura, cond-mat/0108276, submitted to Phys. Rev. Lett.
22) A. Sugita, K. Arita and K. Matsuyanagi, Prog. Theor. Phys. **100** (1998), 597.
23) K. Arita, A. Sugita and K. Matsuyanagi, Prog. Theor. Phys. **100** (1998), 1223.
24) A. G. Magner, S. N. Fedotkin, K. Arita, K. Matsuyanagi and M. Brack, Phys. Rev. E **63** (2001), 065201(R).
25) H. Nishioka, M. Ohta and S. Okai, Mem. Konan Univ. Sci. Ser. **38** (2) (1991), 1 (unpublished).
26) H. Nishioka, N. Nitanda, M. Ohta and S. Okai, Mem. Konan Univ. Sci. Ser. **39** (2) (1992), 67 (unpublished).
27) K. Arita, A. Sugita and K. Matsuyanagi, *Proc. Int. Conf. on "Atomic Nuclei and Metallic Clusters", Prague, 1997*, Czech. J. of Phys. **48** (1998), 821.
28) A. G. Magner, S. N. Fedotkin, K. Arita, K. Matsuyanagi, T. Misu, T. Schachner and M. Brack, Prog. Theor. Phys. **102** (1999), 551.
29) S. C. Creagh, Ann. of Phys. **248** (1997), 60.
30) S. Tomsovic, M. Grinberg and D. Ullmo, Phys. Rev. Lett. **75** (1995), 4346.
D. Ullmo, M. Grinberg and S. Tomsovic, Phys. Rev. E **54** (1996), 136.
31) M. Sieber, J. of Phys. A **30** (1997), 4563.
32) P. J. Richens, J. of Phys. A **15** (1982), 2110.
33) P. Meier, M. Brack and C. Creagh, Z. Phys. D **41** (1997), 281.
34) H. Waalkens, J. Wiersig and H. R. Dullin, Ann. of Phys. **260** (1997), 50.
35) M. Sieber, J. of Phys. A **29** (1996), 4715.
36) H. Schomerus and M. Sieber, J. of Phys. A **30** (1997), 4537.
M. Sieber and H. Schomerus, J. of Phys. A **31** (1998), 165.
37) M. Brack, P. Meier and K. Tanaka, J. of Phys. A **32** (1999), 331.
38) C. Chester, B. Friedmann and F. Ursell, Proc. Cambridge Philos. Soc. **53** (1957), 599.
39) M. V. Fedoryuk, Sov. J. of Comp. Math. and Math. Phys. **4** (1964), 671; ibid. **10** (1970), 286.
40) A. D. Bruno, preprint Inst. Prikl. Mat. Akad. Nauk SSSR Moskva (1970), 44 (in Russian).
41) V. P. Maslov, Theor. Math. Phys. **2** (1970), 30.
42) M. V. Fedoryuk, *Saddle-point method* (Nauka, Moscow, 1977, in Russian).
43) M. V. Fedoryuk, *Asymptotics: Integrals and sums* (Nauka, Moscow, 1987, in Russian).
44) V. M. Strutinsky, Nucl. Phys. A **122** (1968), 1; and earlier references quoted therein.
45) M. Brack et al., Rev. Mod. Phys. **44** (1972), 320.
46) M. Abramowitz and I. A. Stegun, *Handbook of mathematical functions* (Dover publications INC., New York, 1964).
47) Paul F. Byrd and Morris D. Friedman, *Handbook of Elliptic Integrals for Engineers and Scientists* (Springer-Verlag, 1971).
48) L. D. Landau and E. M. Lifshits, *Theoretical Physics, Vol. 1, Classical mechanics* (Nauka, Moscow, 1973, in Russian).
49) I. S. Gradshteyn and I. M. Ryzhik, *Tables of integrals, series, and products, 6th ed.* (Academic Press, 2000).
50) T. Mukhopadhyay and S. Pal, Nucl. Phys. A **592** (1995), 291.